nature communications

Article

https://doi.org/10.1038/s41467-025-59090-w

SAMD9 senses cytosolic double-stranded nucleic acids in epithelial and mesenchymal cells to induce antiviral immunity

Received: 25 November 2024

Accepted: 11 April 2025

Published online: 22 April 2025

Check for updates

Gaopeng Hou[1], Wandy Beatty[1], Lili Ren[2,3,4,5], Yaw Shin Ooi[3,11], Juhee Son[1], Yinxing Zhu[1], Qingyu Sheng[6], Wanyi Huang[1], Dian Li[7], Constin Liu[1], Olivia L. Welsh[8,9], Danica M. Sutherland[8,9], Terence S. Dermody[8,9], Chen Shen[6], Jia Liu[10], L. David Sibley[1] & Siyuan Ding[1]

Sensing of cytosolic, double-stranded (ds) DNA or dsRNA molecules derived from microbial or endogenous sources triggers cell-intrinsic innate immunity, but sensors recognizing both cytosolic dsDNA and dsRNA are sparsely reported. Here we find that full-length human SAMD9 protein directly binds to synthetic or viral dsDNA or dsRNA. Overexpression of SAMD9 from various vertebrate species leads to robust production of interferons and pro-inflammatory cytokines. By contrast, loss of endogenous SAMD9 impairs the interferon responses to cytosolic dsDNA and dsRNA stimulation in multiple cell types and enhances the infectivity of pathogenic dsDNA and dsRNA viruses. Mice lacking *Samd9l*, the human SAMD9 homolog, show increased viral load and severe clinical manifestations of rotavirus and reovirus infections. Rotavirus-encoded non-structural protein 1 targets SAMD9 for proteasomal degradation. Collectively, our data demonstrate that SAMD9 may serve as a pattern-recognition receptor for cytosolic dsDNA and dsRNA across different domains of life and represents a potential target of viral innate immune evasion.

Host innate immunity provides the first line of defense against invading microbial pathogens through germline-encoded pattern-recognition receptors (PRRs) that detect pathogen-associated molecular patterns (PAMPs)[1,2]. Cytosolic double-stranded (ds) DNA is sensed by cyclic GMP-AMP synthase (cGAS)[3], which produces 2′3′ cyclic GMP-AMP, a second messenger that activates an endoplasmic-reticulum-resident adaptor protein, stimulator of interferon genes (STING), and subsequent interferon (IFN) responses[4]. In contrast, cytosolic dsRNA molecules are recognized by RIG-I-like receptors (RLRs), including retinoic acid-inducible gene I (RIG-I)[5] and melanoma differentiation-associated protein 5 (MDA5)[6]. RIG-I preferentially binds to uncapped RNA bearing a triphosphate group[7] or a diphosphate group[8], while MDA5 recognizes long dsRNA[9]. Both RIG-I and MDA5 oligomerize following substrate binding and signal using the adaptor protein, mitochondria antiviral-signaling protein (MAVS), to induce IFN expression[10–13]. In addition to cGAS and RLRs, several other cytosolic

[1]Department of Molecular Microbiology, Washington University School of Medicine in St. Louis, St. Louis, MO, USA. [2]Department of Medicine, Division of Gastroenterology and Hepatology, Stanford University, Stanford, CA, USA. [3]Department of Microbiology and Immunology, Stanford University, Stanford, CA, USA. [4]Palo Alto Veterans Institute of Research, VA Palo Alto Health Care System, Palo Alto, CA, USA. [5]School of Pharmaceutical Sciences, Nanjing Tech University, Nanjing, China. [6]Division of Infectious Diseases, Department of Medicine, Washington University School of Medicine in St. Louis, St. Louis, MO, USA. [7]Division of Nephrology, Department of Medicine and Department of Developmental Biology, Washington University in St. Louis, St. Louis, MO, USA. [8]Department of Pediatrics, University of Pittsburgh School of Medicine, Pittsburgh, PA, USA. [9]Institute of Infection, Inflammation, and Immunity, UPMC Children's Hospital of Pittsburgh, Pittsburgh, PA, USA. [10]Department of Microbiology and Immunology, University of Arkansas for Medical Sciences, Little Rock, AR, USA. [11]Present address: Emerging Infectious Diseases Program, Duke-NUS Medical School, Singapore, Singapore. e-mail: siyuan.ding@wustl.edu

dsDNA or dsRNA sensors mediate inflammasome activation or serve as regulators of IFN signaling[14–18]. Activation of these innate immune response by microbial derived dsDNA or dsRNA not only controls initial infection but also shapes adaptive immunity[1]. Despite extensive investigation of the innate immune sensing of cytosolic dsDNA and dsRNA, with the exception of ZBP1, which recognizes noncanonical Z-form nucleic acids[19,20], common sensors for dsDNA and dsRNA have not been reported.

Sterile Alpha Motif Domain-containing 9 (SAMD9) is an IFN-stimulated gene (ISG)[21] that encodes an eponymous N-terminal SAM domain that potentially mediates oligomerization[22], an AlbA domain capable of nucleic acid binding[23], a putative STAND-like P-loop NTPase domain[24], and an oligonucleotide binding (OB)-fold domain also with nucleic acid binding ability[24]. SAMD9 restricts poxvirus infection[25,26] and is antagonized by poxvirus-encoded factors[25,27]. SAMD9 is evolutionarily conserved[28], and mutations in human *SAMD9* cause a severe multi-system disorder called the MIRAGE (myelodysplasia, infection, restriction of growth, adrenal hypoplasia, genital phenotypes, and enteropathy) syndrome[29]. Interestingly, the mouse genome lacks a direct ortholog of human SAMD9 and instead encodes only SAMD9-like gene *Samd9l*[30].

Rotaviruses and reoviruses are members of the dsRNA virus family *Sedoreoviridae* and cause significant gastrointestinal and systemic diseases in infants and young animals worldwide[31,32]. Despite the availability of vaccines, rotavirus remains a leading cause of severe pediatric diarrhea globally, especially in developing countries[33], and reoviruses are studied extensively as models of viral pathogenesis and antiviral immunity[34]. Both viruses use dsRNA as the genetic material and generate more cytosolic dsRNA during replication[35,36], triggering host innate immune responses, but they also employ diverse strategies to evade or antagonize these defenses[37,38].

In this study, we directly investigate whether SAMD9 serves as a shared innate immune sensor for surveillance of both cytosolic dsDNA and dsRNA and functions as a broad-spectrum antiviral host protein. Using a combinatorial approach of unbiased screens, organoid cultures, and animal models, we find that SAMD9 binds to both dsDNA and dsRNA, oligomerizes upon nucleic acid binding, and initiates IFN signaling through the MAVS-TBK1-IRF3 axis. We also identify rotavirus non-structural protein 1 (NSP1) as a viral antagonist that degrades SAMD9, revealing a novel mechanism of viral immune evasion. These findings establish SAMD9 as a critical innate immune sensor of both dsDNA and dsRNA and significantly expand our understanding of virus-host arms race.

Results

SAMD9 expression activates IFN signaling

To gain insights into the cytoplasmic nucleic acid sensing, we conducted a biochemical affinity screen to identify cytoplasmic proteins that bind both canonical dsDNA and dsRNA (Supplementary Fig. 1A). SAMD9 emerged as a top candidate for this dual functionality (Supplementary Fig. 1B–D and Supplementary Data 1). We first determined whether SAMD9 acts as a functional innate immune sensor for both cytosolic dsDNA and dsRNA. Several cytosolic sensors, such as MDA5, are ISGs and thus drive a positive feedback loop of IFN production when overexpressed[39]. Using RNA sequencing, we compared the global transcriptomes of SAMD9-overexpressing and empty vector-transfected A549 cells. Type I and type III IFNs, multiple canonical ISGs, such as MX1 and ISG15, and several pro-inflammatory cytokines, including CCL5 and CXCL10, were among the most strongly induced genes following SAMD9 overexpression (Fig. 1A). We confirmed by qRT-PCR that mRNA levels of type I and III IFNs, CCL5, CXCL10, and MX1, were highly induced in SAMD9-overexpressing cells (Fig. 1B and Supplementary Fig. 2A–C), and enhanced secretion of IFN-λ3 and CCL5 proteins was verified by ELISA (Fig. 1C, D). A K350A SAMD9 mutant that is defective in binding to phenylalanine tRNA[40] still induced high levels of IFNL3 expression (Supplementary Fig. 2D), suggesting that the IFN induction phenotype is distinct from the afore-published tRNA binding and cleavage. SAMD9-induced IFN and CCL5 expression was also observed in HEK293 cells (Supplementary Fig. 3). SAMD9-activated signaling was not mediated by sensing of transfected SAMD9 plasmids by the cytosolic STING pathway, as comparable expression of IFNL3 and CCL5 was detected in *STING* knockout (KO) A549 cells (Supplementary Fig. 4A–C) and STING inhibitor H-151[41] treated cells (Supplementary Fig. 4D, E). Instead, IFN induction seemed to rely on MAVS, TBK1 (Fig. 1E–G) and IRF3 (Supplementary Fig. 4A–C). In contrast to RNA polymerase III inhibitor ML-60218[42], a dual inhibitor of TBK1 and IKKε BX-795[43] also reduced IFN and CCL5 expression (Supplementary Fig. 4D, E). Consistent with these data, we observed strong IRF3 phosphorylation and nuclear translocation in SAMD9-overexpressing cells (Fig. 1H and Supplementary 4F). Additionally, ruxolitinib, a JAK1/2 inhibitor[44], completely blocked MX1 expression induced by IFN-α or IFN-λ treatment (Supplementary Fig. S4G), while SAMD9 overexpression in the presence of ruxolitinib still induced high levels of IFNL3 and CCL5 (Fig. 1I, J). Based on these findings, we continued to investigate a potentially new SAMD9-mediated innate immune signaling pathway.

Endogenous SAMD9 mediates IFN induction by cytosolic dsDNA and dsRNA

To assess the function of endogenous SAMD9 as a PRR, we generated clonal CRISPR/Cas9 *SAMD9* KO, *RIG-I* KO, *RIG-I SAMD9* double KO, *MDA5* KO, *MDA5 SAMD9* double KO, *RIG-I MDA5* double KO, *RIG-I MDA5 SAMD9* triple KO, *MAVS* KO[37], *MAVS SAMD9* double KO, *STING* KO, and *STING SAMD9* double KO in HT-29 cells. These cells were validated by Sanger sequencing and cross-examined for expression of other sensors by immunoblotting (Supplementary Fig. 5 and Fig. 2A, B). *SAMD9* KO cells were also complemented by reintroducing a C-terminally mGFP-tagged version of SAMD9 (Supplementary Fig. 5C). As expected, transfection of polydeoxyadenylic-deoxythymidylic acid (poly(dA:dT)), a B-form synthetic dsDNA, stimulated high levels (~167-fold induction) of IFNL3 expression in wild-type (WT) HT-29 cells (Fig. 2C). The IFN induction levels were decreased to 37-fold in *SAMD9* KO cells, representing a ~80% reduction, similar to that observed using *STING* KO HT-29 cells, and IFN levels were restored in *SAMD9* KO HT-29 cells complemented with SAMD9 (Fig. 2C). Additionally, IFNL3 induction levels were significantly reduced (~77%) in *STING SAMD9* double KO cells, compared to *STING* KO HT-29 cells (Fig. 2C). We observed a similar trend using herring testes DNA (HT-DNA), another immunostimulatory cytosolic dsDNA ligand (Supplementary Fig. 6A). Likewise, stimulation with polyinosinic-polycytidylic acid (poly(I:C)), an A-form viral dsRNA mimic, triggered high levels (~220-fold induction) of IFNL3 expression in WT HT-29 cells, while IFN expression in *SAMD9* KO cells were reduced by ~90% (Fig. 2D). Importantly, poly(I:C) transfection stimulated ~17-, ~82-, and ~3.3-fold induction of IFNL3 expression in *RIG-I* KO, *MDA5* KO, *RIG-I MDA5* double KO HT-29 cells; however, these values were further reduced by an additional ~65%, ~90%, and ~100%, respectively, if *SAMD9* was knocked out in these cell lines (Fig. 2D). In *MAVS* KO HT-29 cells, the induction of IFNL3 was completely abrogated, and the addition of *SAMD9* KO did not have an impact (Fig. 2D). In comparison, IFNL3 and CCL5 induction by polyuridine (polyU), a single-stranded RNA (ssRNA) mimic, a TLR7 antagonist[45], was not affected by the loss of SAMD9 (Supplementary Fig. 6B, C). Dampened IFN and CCL5 induction in response to poly(dA:dT) and poly(I:C) was independently validated using *SAMD9* KO HEK293 and *SAMD9* KO A549 cells (Supplementary Figs. 7 and 8). It is important to note that the expression of IFN and CCL5 was not completely returned to the baseline levels in *SAMD9* KO cells, suggesting that it is not the only sensor in these cells. Because SAMD9 is ubiquitously expressed in many human tissues and cell types (Supplementary Fig. 9A), we sought to establish the relevance of *SAMD9* in cytosolic dsDNA and dsRNA

https://doi.org/10.1038/s41467-025-59090-w

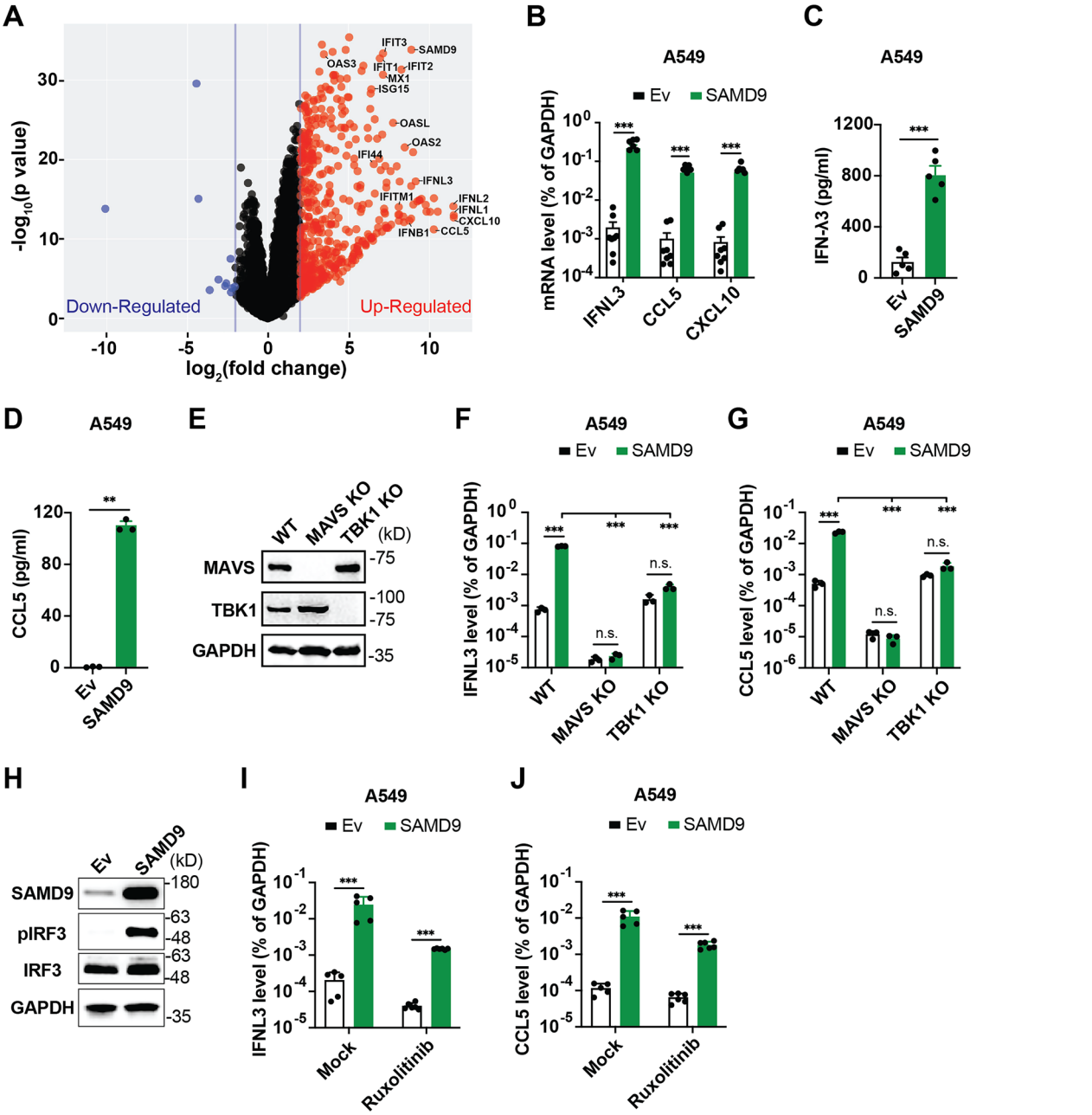

Fig. 1 | SAMD9 overexpression activates IFN signaling in a MAVS-TBK1-IRF3 dependent manner. A A volcano plot of RNA sequencing results indicating top gene transcripts upregulated (red) and downregulated (blue) by SAMD9 overexpression as compared to empty vector (Ev) transfection in A549 cells. **B**–**D** A549 cells transfected with Ev or SAMD9-Myc-DDK plasmid for 24 h and the mRNA levels of IFNL3, CCL5, and CXCL10 measured by qRT-PCR (**B**), and levels of secreted IFN-λ3 (**C**) or CCL5 (**D**) quantified by ELISA. **E** Validation of wild-type (WT), single clonal *MAVS* KO, *TBK1* KO A549 cells by western blot with indicated antibodies. **F**, **G** WT, single clonal *MAVS* KO and *TBK1* KO A549 cells transfected with Ev or SAMD9-Myc-DDK plasmid for 24 h and the mRNA levels of IFNL3 (**F**) and CCL5 (**G**) measured by qRT-PCR. **H** A549 cells transfected with Ev or SAMD9-Myc-DDK plasmid for 24 h, and cell lysates harvested for SDS-PAGE electrophoresis with indicated antibodies. **I**, **J** A549 cells incubated with ruxolitinib (10 μM) for 1 h, transfected with Ev or SAMD9-Myc-DDK for 24 h and the mRNA levels of IFNL3 (**I**) and CCL5 (**J**) measured by qRT-PCR. The RNA sequencing experiment in (**A**) was performed once in duplicate, other experiments were repeated at least three times. Individual points in (**B**–**D**, **F**, **G**, **I**, and **J**) represent independent experiments. Data are represented as mean ± SEM. Statistical significance calculated by two-way ANOVA with Sidak's multiple-comparisons tests (**B**, **F**, **G**, **I**, and **J**), or unpaired two-tailed Student's *t*-test (**C**, **D**): n.s., not significant, $^{*}P < 0.05$, $^{**}P < 0.01$, $^{***}P < 0.001$. Source data are provided as a Source Data file. Detailed *P*-values are provided in the Source Data file.

sensing in non-transformed human cells. Indeed, IFN production was significantly impaired in poly(dA:dT)- and poly(I:C)-stimulated primary human intestinal organoids lacking SAMD9 (Fig. 2E–G), and primary human hepatocytes (Fig. 2H, I), as well as in poly(I:C)-transfected primary human cardiomyocytes (Supplementary Fig. 9B, C) and primary adult human dermal fibroblasts (Supplementary Fig. 9D, E), but not in human monocytic THP-1 cells (Supplementary Fig. 9F, G), highlighting potential cell type-specific sensing by SAMD9.

SAMD9 binds to dsDNA and dsRNA

To distinguish whether SAMD9 acts as a sensor by itself or positively regulates RIG-I and cGAS signaling as previously reported[46], we next

https://doi.org/10.1038/s41467-025-59090-w

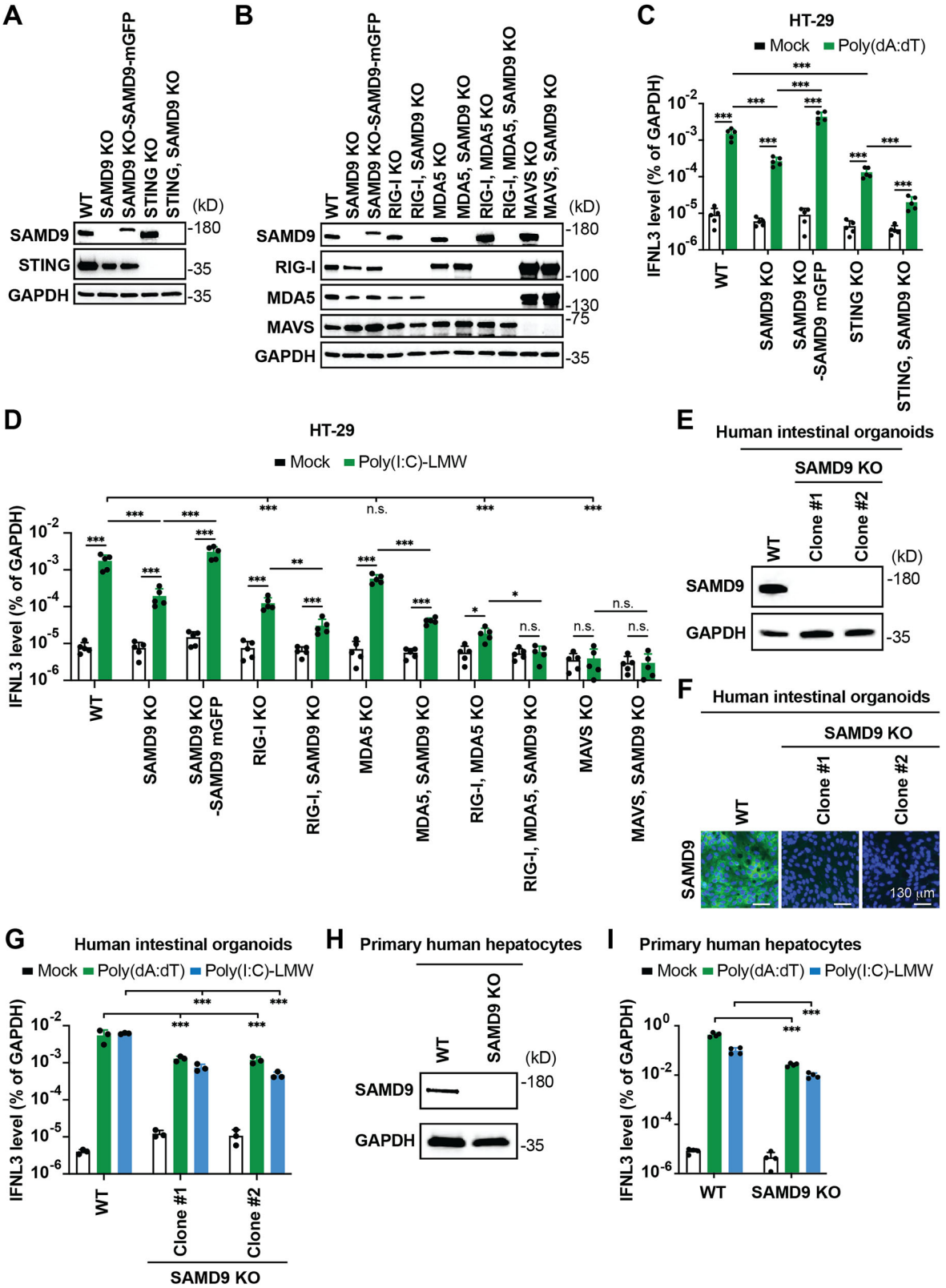

evaluated if SAMD9 directly binds to dsDNA and/or dsRNA. We purified recombinant full-length (~180 kD) human SAMD9 proteins using baculoviruses and insect cell expression systems (Fig. 3A). In electrophoretic mobility shift assays, we found strong binding of human SAMD9 to circular dsDNA (Supplementary Fig. 10A). The binding was SAMD9 dose-dependent (Fig. 3B) with an estimated dissociation constant (Kd) of ~77 nM, calculated based on a half-maximum binding on a curve fit (Fig. 3C). SAMD9 also bound to poly(dA:dT) (Supplementary Fig. 10B). Additionally, SAMD9 bound to linear dsDNA molecules ranging from 40 bp to 1280 bp (Fig. 3D and Supplementary Fig. 10C) but not 15-bp and 20-bp dsDNA (Fig. 3D) or 80-bp single-stranded DNA (Fig. 3E), suggesting that SAMD9-dsDNA interactions occur in a length-dependent but sequence-independent manner. SAMD9 also bound to dsRNA molecules of different sizes. Poly(I:C), of either low (0.2–1 kb) or high

Fig. 2 | SAMD9 senses cytosolic dsDNA and dsRNA. A Validation of WT, *SAMD9* KO, SAMD9-mGFP add-back *SAMD9* KO, *STING* KO, *STING SAMD9* double KO HT-29 cells by western blot with indicated antibodies. **B** WT, *SAMD9* KO, *SAMD9* KO complemented with SAMD9-mGFP, *STING* KO, and *STING SAMD9* double KO HT-29 cells transfected with poly(dA:dT) (1 μg/ml) for 24 h and the IFNL3 mRNA level measured by qRT-PCR. **C** Validation of WT, *SAMD9* KO, SAMD9-mGFP add-back *SAMD9* KO, *RIG-I* KO, *RIG-I SAMD9* double KO, *MDA5* KO, *MDA5 SAMD9* double KO, *RIG-I MDA5* double KO, *RIG-I MDA5 SAMD9* triple KO, *MAVS* KO, *MAVS SAMD9* double KO HT-29 cells by western blot with indicated antibodies. **D** WT, *SAMD9* KO, *SAMD9* KO complemented with SAMD9-mGFP, *RIG-I* KO, *RIG-I SAMD9* double KO, *MDA5* KO, *MDA5 SAMD9* double KO, *RIG-I MDA5* double KO, *RIG-I MDA5 SAMD9* triple KO, *MAVS* KO, and *MAVS SAMD9* double KO HT-29 cells transfected with LMW poly(I:C) (1 μg/ml) for 24 h and the IFNL3 mRNA level measured by qRT-PCR. **E**, **F** Validation of WT and two individual single clonal *SAMD9* KO human intestinal organoids by western blot (E) and immunofluorescence staining **F**. **G** WT and two individual *SAMD9* KO clones of human ileal organoids transfected with poly(dA:dT) or LMW poly(I:C) (1 μg/ml) for 24 h and the IFNL3 mRNA level measured by qRT-PCR. Human ileal organoids fixed and stained for SAMD9 (green) and nuclei (blue) by microscopy. **H** Validation of WT and *SAMD9* KO primary human hepatocytes by western blot. **I** IFNL3 mRNA levels in poly(dA:dT) or LMW poly(I:C) (1 μg/ml) transfected WT and *SAMD9* KO primary human hepatocytes measured by qRT-PCR. For all figures, experiments were repeated at least three times. Individual points in (**B**, **D**, **G**, and **I**) represent independent experiments. Data are represented as mean ± SEM. Statistical significance calculated by two-way ANOVA with Tukey's multiple-comparisons tests (**B**, **D**, **G**, and **I**): n.s., not significant, $^{*}P < 0.05$, $^{**}P < 0.01$, $^{***}P < 0.001$. Source data are provided as a Source Data file. Detailed *P*-values are provided in the Source Data file.

(1.5–8 kb) molecular weight, shifted to a higher relative molecular weight following SAMD9 binding (Supplementary Fig. 10D). Moreover, SAMD9 bound to linear dsRNA molecules ranging from 42 bp to 512 bp (Fig. 3F). However, SAMD9 did not bind to 16-bp and 20-bp dsRNA (Fig. 3F) or polyU ssRNA (Fig. 3G). SAMD9 bound to 512-bp linear dsRNA with an estimated Kd of ~185 nM (Fig. 3H, I). Analogous to cGAS, RIG-I, and MDA5, which form dimeric or oligomeric structures during ligand binding[47–50], SAMD9 also oligomerized when incubated with dsDNA under non-denaturing conditions (Supplementary Fig. 10E). By negative stain electron microscopy, we visualized two types of higher-order SAMD9-dsDNA complexes, assuming either filament-like or disc-like structures (Supplementary Fig. 10F).

The OB-fold domain is required for SAMD9 oligomerization and IFN induction

Human SAMD9 encodes an N-terminal AlbA domain, which is known to bind to dsDNA and dsRNA using purified single AlbA domain[23]; and a C-terminal OB-fold domain[24] has been predicted with putative oligonucleotide binding abilities, but neither of which has been studied in the full-length protein. Since there is no functional evidence linking the OB-fold domain to nucleic acid sensing or IFN signaling, we complemented *SAMD9* KO HT-29 cells with mGFP-tagged full-length or OB-deletion (ΔOB) SAMD9 constructs (Fig. 4A, B). Relative to the full-length SAMD9, the ΔOB mutant was incapable of restoring IFNL3 induction in *SAMD9* KO HT-29 cells in response to poly(dA:dT) or poly(I:C) stimulation (Fig. 4C, D). To determine the mechanism of attenuated IFN activation by the ΔOB mutant, we purified recombinant SAMD9 ΔOB protein and tested the capacity of the recombinant protein to bind dsDNA using an EMSA assay. SAMD9 ΔOB protein bound to circular dsDNA with comparable affinity than the full-length protein (Fig. 4E). AlbA domain was not responsible for the nucleic acid binding in the SAMD9 ΔOB protein because recombinant SAMD9 protein without both AlbA and OB domains (ΔAlbA+OB) still bound to dsDNA (Supplementary Fig. 11A). We conducted two additional immunoprecipitation experiments to examine SAMD9-DNA interactions. First, cell lysates containing full-length or ΔOB SAMD9 were incubated with biotinylated dsDNA followed by streptavidin immunoprecipitation. Second, Flag-tagged SAMD9 constructs were immunoprecipitated using anti-Flag antibodies, followed by DNA electrophoresis. In both cases, OB deletion had little to no impact on the dsDNA binding activity of SAMD9 (Fig. 4F, G). Biotinylated dsDNA immunoprecipitation assay with cell lysates containing ΔAlbA or ΔAlbA+OB SAMD9 showed that neither of the AlbA or OB domain is necessary for dsDNA binding (Supplementary Fig. 11B). We next established a cell-based SAMD9 oligomerization assay to determine its activation status following ligand engagement. Similar to observations made using recombinant proteins and dsDNA in vitro (Supplementary Fig. 10E, F), WT SAMD9 and mGFP-tagged SAMD9 in *SAMD9* KO HT-29 cells formed higher-ordered structures when stimulated with poly(dA:dT), as detected by native PAGE gel (Fig. 4H). In contrast, SAMD9 ΔOB in the complemented cells did not oligomerize (Fig. 4H), suggesting that the OB domain is required for SAMD9 oligomerization and IFN activation.

SAMD9 restricts the infection of dsDNA and dsRNA viruses that replicate in the cytosol

To determine whether SAMD9 recognizes natural dsDNA and dsRNA PAMPs, such as those produced during viral infections, we purified the dsRNA genome from rotavirus (RV), which contains 11 distinct dsRNA segments ranging from 600 bp to 3400 bp[51]. SAMD9 strongly bound to RV genomic dsRNAs, and the migration of the large SAMD9-dsRNA complexes was retarded in a gel-shift assay (Fig. 5A). Consistent with its role as a cytosolic nucleic acid PRR, SAMD9 was predominantly detected in the cytoplasmic fraction together with tubulin, but not with nuclei or other membrane-associated organelles (Fig. 5B). Immunostaining of SAMD9 using antibodies purchased from different vendors revealed the same cytoplasmic distribution pattern (Supplementary Fig. 12A). Additionally, super-resolution microscopy showed strong colocalization of SAMD9 with tubulin, confirming its presence in the cytoplasm (Supplementary Fig. 12B). SAMD9 also displayed cytoplasmic localization in primary human ileal organoids that contain differentiated small intestinal epithelial cell types (Supplementary Fig. 12C). RV dsRNA co-localized with endogenous SAMD9 in RV-infected A549 cells (Fig. 5C), as did transfected poly(dA:dT) and poly(I:C) (Supplementary Fig. 13). During RV infection, full-length but not ΔOB SAMD9 formed oligomerized structures (Fig. 5D and Supplementary Fig. 14), similar to those seen with poly(dA:dT) transfection (Fig. 4H). SAMD9 oligomerization occurred concurrently with RIG-I oligomerization, IRF3 phosphorylation and dimerization (Fig. 5D). RV infection induced weak IRF3 phosphorylation in ΔOB SAMD9 complemented cells (Supplementary Fig. 14). In RV-infected A549 cells, SAMD9 was observed in both the viral protein VP6-positive P8000 fraction and the S8000 fraction, which suggests a partial relocalization of activated SAMD9 from cytoplasm to membranous organelles (Supplementary Fig. 15).

We expanded the functional analysis of SAMD9 in IFN induction beyond synthetic dsDNA and dsRNA ligands to natural viral infections. Compared to WT, *RIG-I* KO, *MDA5* KO, and *RIG-I MDA5* double KO HT-29 cells, the lack of SAMD9 in these cells led to a significant reduction of IFNL3 and CCL5 expression following RV infection (Fig. 5E, F). Infection of modified vaccinia virus Ankara (MVA), a dsDNA virus, also resulted in reduced IFNL3 and CCL5 transcription in *SAMD9* KO HT-29 cells (Supplementary Fig. 16A, B). Decreased IFNL3 and CCL5 secretion was confirmed by ELISA (Fig. 5G, H). In contrast, IFNL3 and CCL5 induction by vesicular stomatitis virus (VSV), which is an ssRNA virus, was not affected by SAMD9 (Supplementary Fig. 16C, D). Defects in IFNB and IFNL3 induction were observed in RV-infected *SAMD9* KO cells as early as 3 h post-infection (Supplementary Fig. 16E–G). To define the specificity of the antiviral

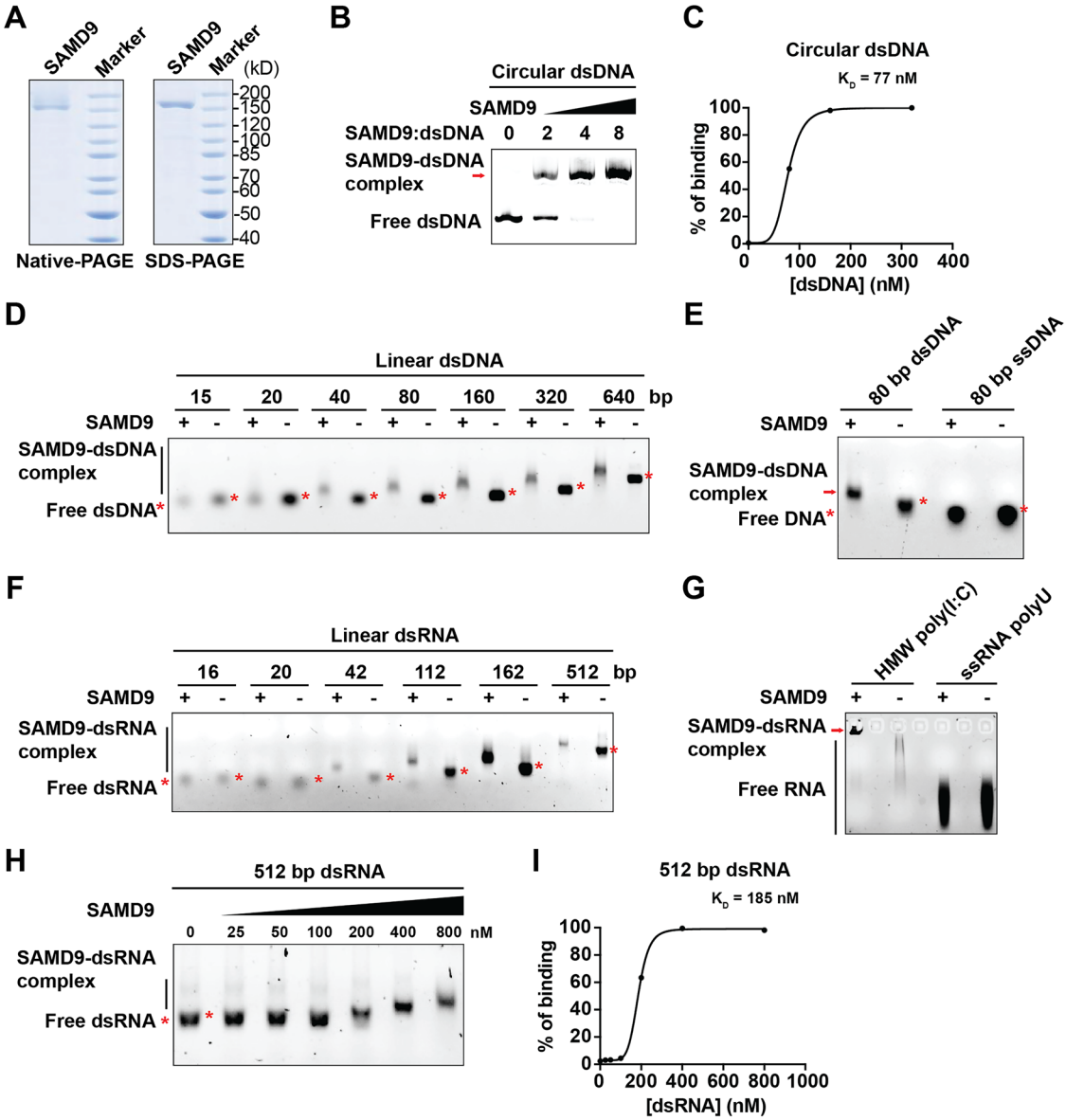

Fig. 3 | SAMD9 binds to dsDNA and dsRNA. A Coomassie stain of His-SAMD9 protein analyzed by native-PAGE (left) or SDS-PAGE (right) electrophoresis. **B** Electrophoretic mobility shift assay (EMSA) of circular plasmid dsDNA with an increasing amount of SAMD9. **C** Measurement of the dissociation constant (K_D) of circular dsDNA with His-SAMD9, calculated based on a half-maximum binding on a curve fit. **D** EMSA of SAMD9 with linear dsDNA fragments of indicated lengths. **E** EMSA of His-SAMD9 with 80-bp dsDNA or 80-bp ssDNA. **F** EMSA of SAMD9 with linear dsRNA fragments of indicated lengths. **G** EMSA of His-SAMD9 with HMW poly(I:C) or single-stranded RNA polyuridine (ssRNA polyU). **H** EMSA of His-SAMD9, provided in 2-fold serial dilutions, with 512-bp dsRNA. **I** K_D measurements of 512 bp dsRNA with His-SAMD9, calculated based on a half-maximum binding on a curve fit. For all figures, experiments were repeated at least three times.

activities of SAMD9, we screened a panel of dsRNA, positive- or negative-sense ssRNA, and dsDNA viruses. Replication of several members of *Sedoreoviridae* (dsRNA viruses, human and animal RVs and mammalian orthoreovirus) and *Poxviridae* (dsDNA viruses) families was enhanced in *SAMD9* KO cells (Fig. 5I), including the emerging monkeypox virus (Supplementary Fig. 17A). In contrast, replication of all ssRNA viruses tested as well as adenovirus and herpes simplex virus type 1, both of which are dsDNA viruses that replicate in the nucleus, was not affected by loss of SAMD9 (Fig. 5I and Supplementary 17B). In addition to intracellular viral RNA levels, titers of RV progeny were approximately 10-fold higher in *SAMD9* KO HT-29 cells, and RV infection was inhibited by reintroduction of either Myc-DDK or mGFP-tagged SAMD9 into *SAMD9* KO HT-29 cells (Supplementary Fig. 17C, D). RV infectivity was also significantly enhanced in single clonal *SAMD9* KO Hela cells[52] (Supplementary Fig. 17E, F).

IFN induction driven by SAMD9 is conserved across different species

SAMD9 and a closely related paralog SAMD9-like protein (SAMD9L) are subjected to positive evolutionary selection[28]. We cloned SAMD9 and SAMD9L homologs from different vertebrate species, including human, mouse, hamster, and zebrafish, into mammalian expression vectors. Compared with SAMD9s that are in close proximity to each other, human SAMD9L shares only 58% amino acid identity with human SAMD9[28] (Fig. 6A). Human SAMD9L is also an ISG[53]. Like SAMD9, human SAMD9L overexpression robustly induced IFNL3 and CCL5 transcription (Fig. 6B–D). However, unlike human SAMD9, human SAMD9L is not readily detectable in most cell types at steady state (Supplementary Fig. 9A), suggesting that human SAMD9 not SAMD9L may function as the PRR during unstimulated and uninfected homeostatic conditions. The common house mouse encodes only a functional *Samd9l* gene[54]. Mouse SAMD9L from two widely used

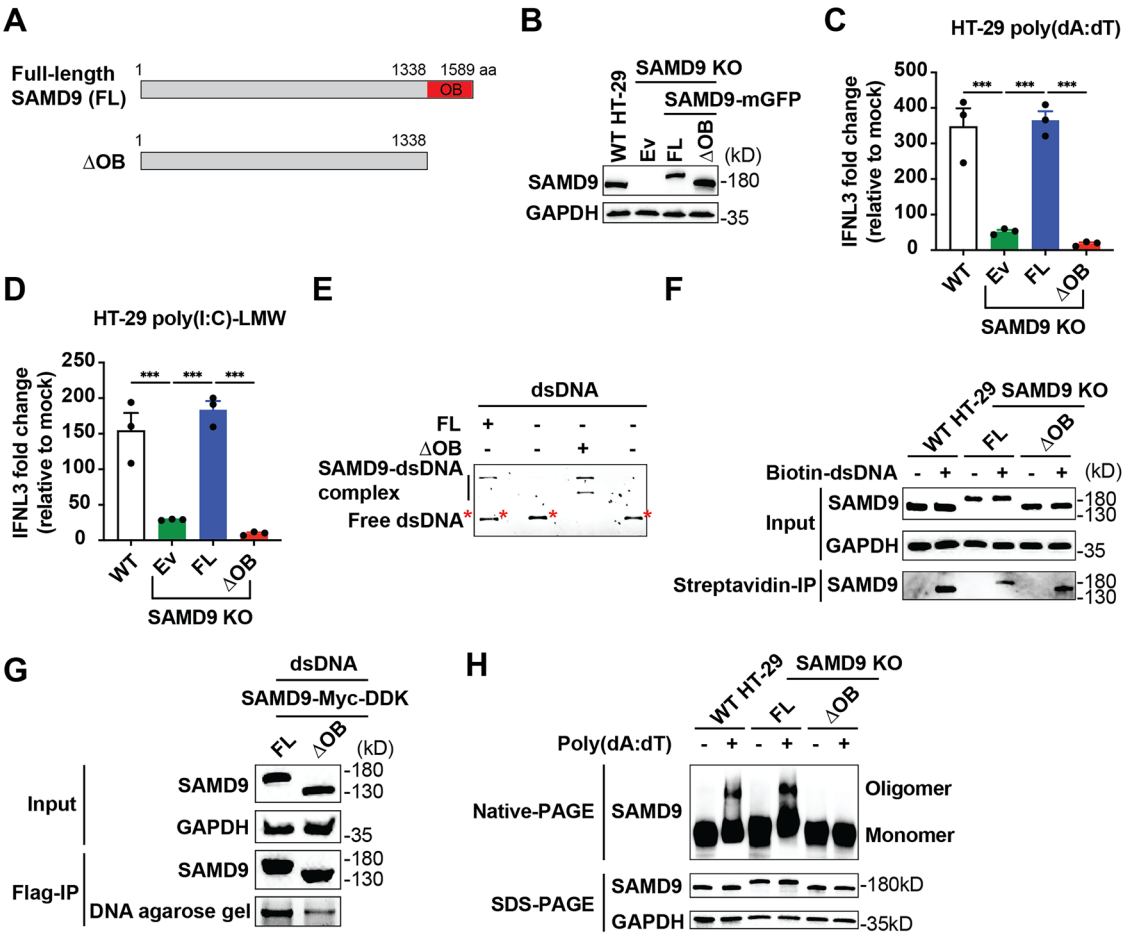

Fig. 4 | SAMD9 OB-fold domain is essential for IFN induction. A Schematic representation of SAMD9. FL full-length, OB oligonucleotide binding-fold domain. **B** Validation of WT HT-29 and *SAMD9* KO HT-29 cells complemented with Ev, SAMD9-mGFP (FL), SAMD9-ΔOB-mGFP (ΔOB) by western blot with indicated antibodies. **C** WT HT-29 and *SAMD9* KO HT-29 cells complemented with Ev, FL, or ΔOB transfected with poly(dA:dT) (1 μg/ml) for 24 h and the IFNL3 mRNA level measured by qRT-PCR. **D** WT HT-29 and *SAMD9* KO HT-29 cells complemented with Ev, FL, or ΔOB transfected with LMW poly(I:C) (1 μg/ml) for 24 h and the IFNL3 mRNA level measured by qRT-PCR. **E** EMSA of His-MBP-tagged SAMD9 FL or ΔOB proteins with circular dsDNA. **F** Immunoblotting analysis of streptavidin immunoprecipitates of cell lysates from WT HT-29 and *SAMD9* KO HT-29 cells complemented with FL or ΔOB incubated with biotinylated 48,502-bp dsDNA. **G** Immunoblotting analysis of anti-Flag antibody immunoprecipitates of cell lysates from HEK293 cells transfected with Myc-DDK-tagged SAMD9 FL or ΔOB. **H** WT HT-29 and *SAMD9* KO HT-29 cells complemented with FL or ΔOB transfected with poly(dA:dT) (10 μg/ml) for 8 h, and cell lysates harvested for native-PAGE or SDS-PAGE electrophoresis with indicated antibodies. For all figures, experiments were repeated at least three times. Individual points in (**C** and **D**) represent independent experiments. Data are represented as mean ± SEM. Statistical significance in (**C** and **D**) calculated by one-way ANOVA with Tukey's post-test: ***$P < 0.001$. Source data are provided as a Source Data file. Detailed *P*-values are provided in the Source Data file.

inbred strains, C57Bl/6J and 129S6/SvEv, differ by two amino acids (V169 and I459)[55], and both induced IFN signaling when overexpressed (Fig. 6E–G). Golden Syrian hamster SAMD9 and SAMD9L and even zebrafish SAMD9L, which is the most divergent of the vertebrate SAMD9 family members tested (Fig. 6A), were capable of inducing high levels of IFNL3 and CCL5 expression (Fig. 6H–J). Since the OB-fold domain of human SAMD9 is required for IFN induction (Fig. 4B–D), we tested the function of the OB-fold domain in human SAMD9L. In wild-type HT-29 cells stably expressing full-length or ΔOB SAMD9L (Supplementary Fig. 18A), OB deletion led to a 3-fold decrease in IFNL3 and CCL5 expression following poly(dA:dT) or poly(I:C) transfection compared with full-length SAMD9L (Supplementary Fig. 18B–E).

Murine Samd9l restricts dsRNA virus infections in vivo

To define the physiological relevance of endogenous SAMD9 in vivo, we generated a new *Samd9l*$^{-/-}$ mouse in the C57Bl/6J background (Supplementary Fig. 19). We isolated crypts that contain intestinal stem cells from WT and *Samd9l*$^{-/-}$ mice to derive primary ileal organoids (Supplementary Fig. 20A, B). Murine Samd9l, like human SAMD9, is abundantly expressed without IFN stimulation (Supplementary Fig. 20B). As expected, IFNL3 induction by RV infection was diminished in *Samd9l*$^{-/-}$ intestinal organoids (Supplementary Fig. 20C), resulting in higher titers of infectious RV (Supplementary Fig. 20D). To test whether Samd9l dampens viral diseases in vivo, we perorally inoculated co-housed *Samd9l*$^{+/+}$ and *Samd9l*$^{-/-}$ littermates with murine RV. Diarrhea occurred in 30% of *Samd9l*$^{-/-}$ mice at 1 day post-infection (dpi), as opposed to 20% in *Samd9l*$^{+/+}$ mice (Supplementary Fig. 20E). As early as at 1 dpi, RV shedding in the feces was increased by more than 10-fold in the absence of murine Samd9l (Supplementary Fig. 20F, G). In a second mouse model of systemic RV dissemination and disease, we perorally inoculated *Samd9l*$^{+/+}$ and *Samd9l*$^{-/-}$ littermates with simian RV. Viral loads in multiple intra- and extra-intestinal tissues, including different segments of the small intestine (*i.e.*, duodenum, jejunum, and ileum), pancreas, and lung, were increased by 10- to 10,000-fold in *Samd9l*$^{-/-}$ mice (Fig. 7A–E). Finally, we tested a third mouse model following lethal infection by mammalian orthoreovirus, which is restricted by SAMD9 in cultured cells (Fig. 5I). Reovirus induces diarrhea and bile-duct obstruction in neonatal mice, as evident

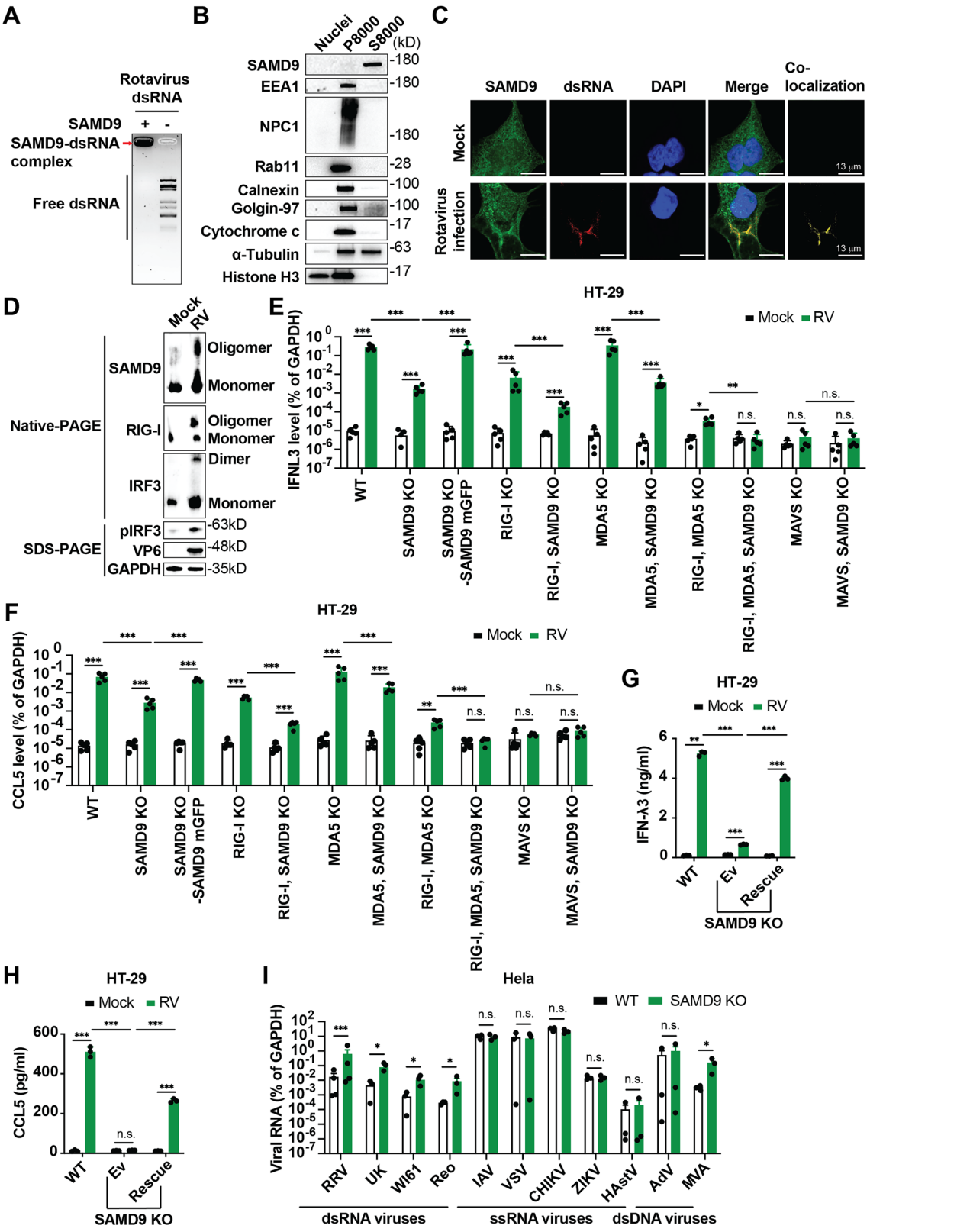

by acholic stool, oily fur, growth retardation[56], and mice eventually succumb to infection. These pathological manifestations were significantly enhanced in the absence of Samd9l. About 70–80% of reovirus-infected *Samd9l*$^{-/-}$ mice developed diarrhea at 3, 4, 7, 8, and 9 dpi, as compared to less than 25% seen in *Samd9l*$^{+/+}$ mice (Fig. 7F). Biliary atresia in *Samd9l*$^{-/-}$ mice appeared at 7 dpi and affected 100% of the animals from 10 to 11 dpi, as opposed to 20% observed in *Samd9l*$^{+/+}$ mice (Fig. 7G), which correlated with reduced mouse survival in *Samd9l*$^{-/-}$ mice (Fig. 7H). Viral loads in the liver, lung, and heart were increased by 10- to 45-fold in *Samd9l*$^{-/-}$ mice (Fig. 7I–K), whereas those in the spleen, kidney, and brain were comparable between *Samd9l*$^{+/+}$ and *Samd9l*$^{-/-}$ mice (Supplementary Fig. 21), again highlighting a potential tissue-specific role of SAMD9 in sensing and antiviral activity. Additionally, we expanded from dsRNA viruses to other sources of

Fig. 5 | SAMD9 restricts the infection of vaccinia virus, rotavirus, and reovirus. **A** EMSA of SAMD9 with rotavirus (RV) segmented dsRNA genome. **B** Nuclear, membrane, and cytoplasmic fractions from A549 cells prepared by homogenization and differential centrifugation. Pellet (P8000) and supernatant (S8000) from centrifugation of 8000×*g* immunoblotted with indicated antibodies. **C** A549 cells infected with mock or RV (MOI = 300) for 8 h, then fixed and stained for SAMD9 (green), dsRNA (red), nuclei (blue) and colocalization (yellow) by confocal microscopy. **D** A549 cells infected with mock or RV (MOI = 3) for 8 h and cell lysates harvested for native-PAGE or SDS-PAGE electrophoresis with indicated antibodies. **E**, **F** WT, *SAMD9* KO, *SAMD9* KO complemented with SAMD9-mGFP, *RIG-I* KO, *RIG-I SAMD9* double KO, *MDA5* KO, *MDA5 SAMD9* double KO, *RIG-I MDA5* double KO, *RIG-I MDA5 SAMD9* triple KO, *MAVS* KO, and *MAVS SAMD9* double KO HT-29 cells infected by RV (MOI = 0.01) for 24 h, the IFNL3 mRNA level (**E**) or CCL5 mRNA level (**F**) measured by qRT-PCR. **G**, **H** WT and *SAMD9* KO complemented with Ev or SAMD9-mGFP (Rescue) HT-29 cells infected with RV (MOI = 0.01) for 24 h, the levels of secreted IFN-λ3 (**G**) and CCL5 (**H**) quantified by ELISA. **I** WT and *SAMD9* KO Hela cells infected by indicated viruses (MOI = 0.1) for 24 h and the mRNA levels of viral genes measured by qRT-PCR. RRV rhesus rotavirus, UK bovine rotavirus, WI61 human rotavirus, Reo mammalian orthoreovirus, IAV influenza A virus, VSV vesicular stomatitis virus, CHIKV chikungunya virus, ZIKV Zika virus, HAstV human astrovirus, AdV adenovirus. For all figures, experiments were repeated at least three times. Individual points in (**E**–**I**) represent independent experiments. Data are represented as mean ± SEM. Statistical significance calculated by two-way ANOVA with Tukey's multiple-comparisons tests (**E**–**I**): n.s., not significant, $^{*}P < 0.05$, $^{**}P < 0.01$, $^{***}P < 0.001$. Source data are provided as a Source Data file. Detailed *P*-values are provided in the Source Data file.

SAMD9 ligands in intestinal organoids. A recent report showed that infection of *Cryptosporidium parvum*, a dsDNA-based eukaryotic pathogen, induces IFNL3 expression in vivo[57], and we found that this IFN induction depends on Samd9l (Supplementary Fig. 22A). TNF-α-induced IFNL3 expression is mediated through mitochondrial dsDNA[58], and also was, at least partially, reduced in *Samd9l*$^{-/-}$ intestinal organoids (Supplementary Fig. 22B), suggesting that SAMD9 is able to recognize endogenous ligands independent of microbial infections. Taken together, these results demonstrate that *Samd9l* contributes to host defense against dsRNA virus infections and accounts for mounting a full-blown IFN response to a variety of host and foreign dsDNA and dsRNA ligands in vivo.

Rotavirus-encoded NSP1 is a viral antagonist of SAMD9

RV encodes several inhibitors of the host innate immune signaling to achieve successful infection[59]. To identify potential RV-encoded viral proteins that can subvert the antiviral function of SAMD9, we systemically examined the impact of all 6 structural proteins and 6 non-structural proteins on endogenous SAMD9 expression. Only NSP1 substantially reduced SAMD9 protein levels (Fig. 8A), without affecting SAMD9 mRNA levels (Supplementary Fig. 23A). To define the role of NSP1 in inhibiting SAMD9 during RV infection, we took advantage of an optimized RV reverse genetics system[60] and generated recombinant RVs with full NSP1 or NSP6 deletion, or C-terminal NSP1 truncation, which is critical for IRF3 binding[61]. SAMD9 protein level was decreased in WT and ΔNSP6 RV-infected cells, but not in ΔNSP1 RV-infected cells (Fig. 8B). Unlike IRF3, SAMD9 protein level was also decreased in cells infected with an RV that lacks the last 17 amino acids of the NSP1 C-terminus (Fig. 8B), suggesting that a motif distinct from IRF3 binding is involved in NSP1 targeting of SAMD9.

GFP-tagged NSP1 co-precipitated with endogenous SAMD9 and IRF3 (Supplementary Fig. 23B). To identify the domain within NSP1 that contributes to SAMD9 binding and decreased SAMD9 protein level, we constructed a series of NSP1 mutants truncated from the C-terminal end (Supplementary Fig. 24A). The region between amino acids 324 and 475 seemed to be important for SAMD9 inhibition (Supplementary Fig. 24B). With additional mutants that we generated (Fig. 8C), we found that NSP1-K474* interacted with SAMD9 and its overexpression decreased SAMD9 protein level (Fig. 8D). In contrast, NSP1-I444* lost the ability to bind and inhibit SAMD9 (Fig. 8D). To define the region of SAMD9 targeted by NSP1, we tested a series of SAMD9 mutants, including the N-terminal SAM and AlbA domains (1–385 aa), the C-terminal OB-fold domain (1170–1589 aa)[52], and internal domains (Fig. 8E and Supplementary Fig. 24C). Neither the 1–385 aa region nor the 1170–1589 aa domain was targeted by NSP1 (Supplementary Fig. 24D, E). We further narrowed down the NSP1 targeting site to SAMD9 388–857 aa region (Fig. 8F), which immunoprecipitated with NSP1 (Fig. 8G). Mechanistically, MLN4924, a NEDD8-activating enzyme inhibitor[62], but not 26S proteasome inhibitors, restored the SAMD9 protein level reduced by NSP1 (Fig. 8H). The involvement of neddylation pathways in SAMD9 protein decrease was also confirmed by siRNA silencing of NEDD8 in NSP1-expressing cells (Fig. 8I). Lastly, we cross-examined SAMD9 or SAMD9L from different species (Fig. 6B–J) with NSP1s derived from different RV strains. NSP1 from two human RV strains preferentially decreased protein levels of SAMD9s while murine RV NSP1 caused significant reduction of SAMD9L protein levels regardless of host species (Fig. 8J and Supplementary Fig. 25). Bovine RV NSP1 only caused decreased protein level of human SAMD9 and the most distant zebrafish SAMD9L was not targeted by any of the human, murine, or bovine RV NSP1s (Fig. 8J and Supplementary Fig. 25), indicating a potential host range restriction of RV infections.

Discussion

In this study, we identify SAMD9 as a PRR that senses both cytosolic dsDNA and dsRNA PAMP molecules. SAMD9 fulfills the criteria of a bona fide sensor: (1) SAMD9 overexpression induces IFN expression and secretion (Fig. 1A–D). (2) Endogenous SAMD9 in epithelial, muscle, and fibroblastic cells mediates IFN expression in response to dsDNA and dsRNA stimulation (Fig. 2 and Supplementary Fig. 9). (3) SAMD9 directly binds to synthetic and viral dsDNA and dsRNA with high affinity (Figs. 3B–I and 5A). (4) SAMD9 oligomerizes following ligand binding (Figs. 4H and 5D). (5) SAMD9 responds to and restricts viral infections in vitro (Fig. 5E–I and Supplementary Fig. 16A, B). (6) SAMD9 is evolutionarily and functionally conserved and at least dates back to zebrafish (Fig. 6), where the IFN systems first emerged. (7) Mouse Samd9l limits RV and reovirus infections in specific organs, such as small intestines, pancreas, liver, lung, and heart, as well as controls diarrhea, biliary diseases, and lethality (Fig. 7).

Although SAMD9 is a restriction factor for myxoma virus (MYXV) and vaccinia virus (VACV)[26,27,63], its exact antiviral mechanism remained elusive. Current models propose that SAMD9 forms stress granules to interfere with viral protein synthesis[63,64], induces tRNA degradation to stall global translation[40], or contributes to IFN responses by acting as a facilitator to promote cGAS sensing in monocytes and macrophages[46]. Our data suggest an alternative explanation that, instead of feeding into cGAS signaling, SAMD9 may directly associate with viral genomes or replication intermediates to activate IFN responses. The induced ISGs include those that stall viral protein translation, such as protein kinase R[65]. Based on this model, it is plausible that poxvirus-encoded factors, including MYXV M062[25] and VACV K1 and C7[66], antagonize SAMD9 by interfering with its dsDNA binding capacity, thereby blocking IFN production. Here, we identified a novel viral antagonist NSP1 encoded by a dsRNA virus. NSP1 seems to interact with SAMD9 in a manner different from MYXV M062 and VACV K1 and C7[25,66] in that NSP1 binds to SAMD9 388–857 aa region while M062 and K1 target the 1–385 aa and 600–1172 aa domain, separately[52,67]. Another major distinction is that NSP1 mediates SAMD9 protein level reduction to interfere with its dsRNA sensing ability, instead of binding and sequestration, a different mode of action employed by poxvirus-encoded factors[63].

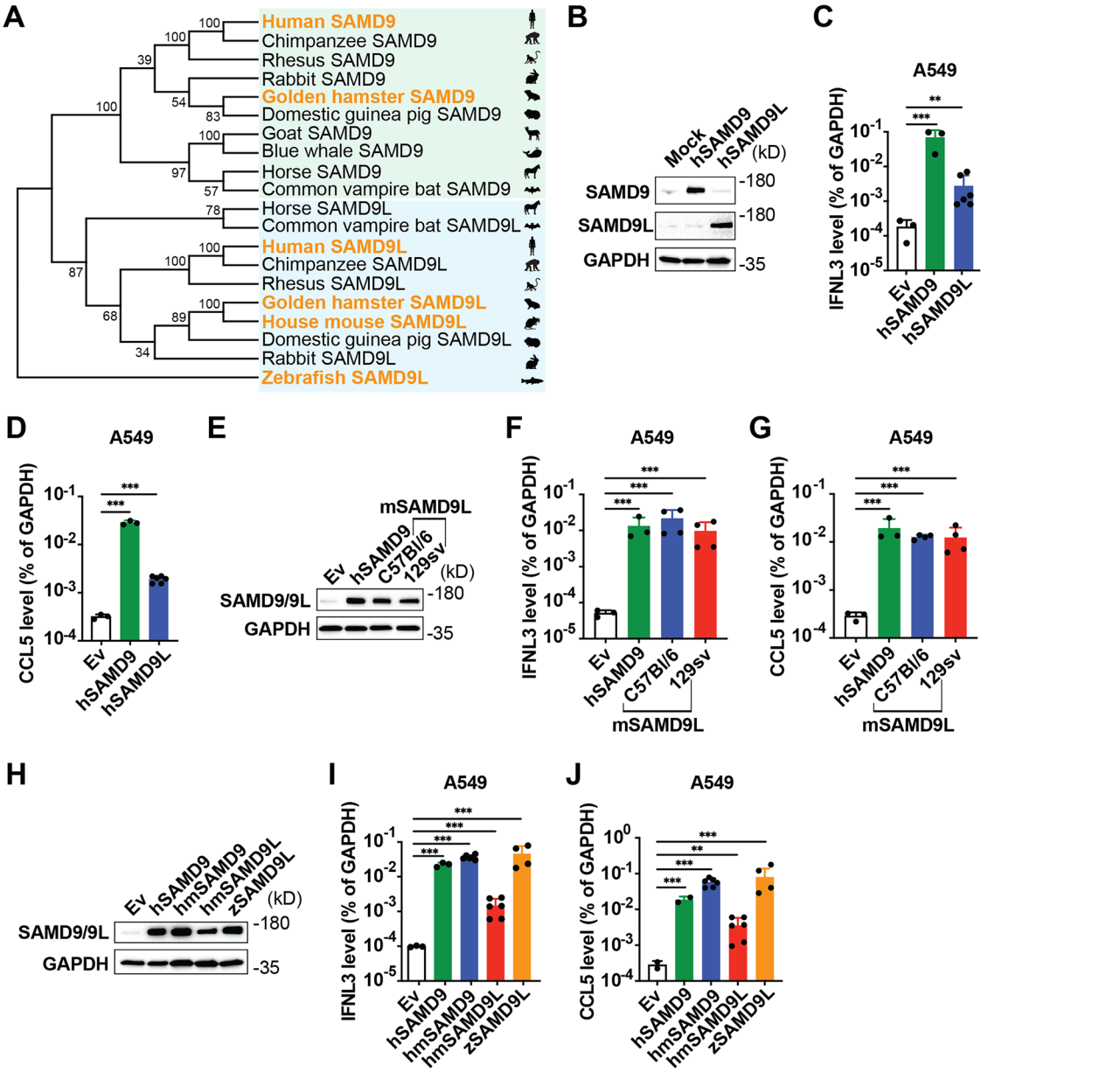

Fig. 6 | SAMD9 from different vertebrate species mediates IFN induction. **A** Maximum likelihood tree of SAMD9 and SAMD9L from selected vertebrate species with bootstrap values indicated on the branches. **B** A549 cells transfected with Ev, human SAMD9 (hSAMD9), and human SAMD9L (hSAMD9L) for 24 h, the SAMD9 and SAMD9L protein levels examined by western blot with indicated antibodies. **C**, **D** A549 cells transfected with Ev, hSAMD9, and hSAMD9L for 24 h, the IFNL3 mRNA level (**C**) and CCL5 mRNA level (**D**) measured by qRT-PCR. **E** A549 cells transfected with Ev, hSAMD9, C57Bl/6J mSAMD9L, and 129S6/SvEv mSAMD9L for 24 h, the SAMD9 and SAMD9L protein levels examined by western blot with indicated antibodies. **F**, **G** A549 cells transfected with Ev, hSAMD9, mSAMD9L from C57Bl/6J or 129S6/SvEv strains for 24 h, the IFNL3 mRNA level (**F**) and CCL5 mRNA level (**G**) measured by qRT-PCR. **H** A549 cells transfected with Ev, hSAMD9, hamster SAMD9 (hmSAMD9), hamster SAMD9L (hmSAMD9L), or zebrafish SAMD9L (zSAMD9L) for 24 h, the SAMD9 and SAMD9L protein levels examined by western blot with indicated antibodies. **I**, **J** A549 cells transfected with Ev, hSAMD9, hmSAMD9, hmSAMD9L, or zSAMD9L for 24 h, the IFNL3 mRNA level (**I**) and CCL5 mRNA level (**J**) measured by qRT-PCR. For all figures, experiments were repeated at least three times. Individual points in (**C**, **D**, **F**, **G**, **I**, and **J**) represent independent experiments. Data are represented as mean ± SEM. Statistical significance calculated by one-way ANOVA with Dunnett's post-test (**C**, **D**, **F**, **G**, **I**, and **J**): $^{*}P < 0.05$, $^{**}P < 0.01$, $^{***}P < 0.001$. Source data are provided as a Source Data file. Detailed *P*-values are provided in the Source Data file.

Although our data support a role of MAVS and TBK1 in IFN induction by SAMD9 either overexpressed (Fig. 1F, G, Supplementary Fig. 4D, E) or at endogenous levels (Figs. 2C, D and 5E, F), the precise mechanisms of IFN activation following SAMD9 nucleic acid binding are not yet clear. However, an emerging theme in mammalian innate immunity, including the RLR and cGAS-STING signaling pathways, is dependence on intact cytoskeletal organization and remodeling[68,69]. The co-segregation and colocalization of SAMD9 with tubulin (Fig. 5B and Supplementary Fig. 12B) suggest the possibility that microtubules and the microtubule-organizing centers are involved in SAMD9-mediated IFN activation. Our future studies will identify the relevant domains of SAMD9 responsible for association with tubulin and nucleic acids and define the functional importance of these interactions.

SAMD9 and SAMD9L from different vertebrate species, including zebrafish, can induce IFN responses in human cells (Fig. 6 and Supplementary Fig. 18A–C). This is surprising, as human SAMD9 and zebrafish SAMD9L share only 29% amino acid identity. However,

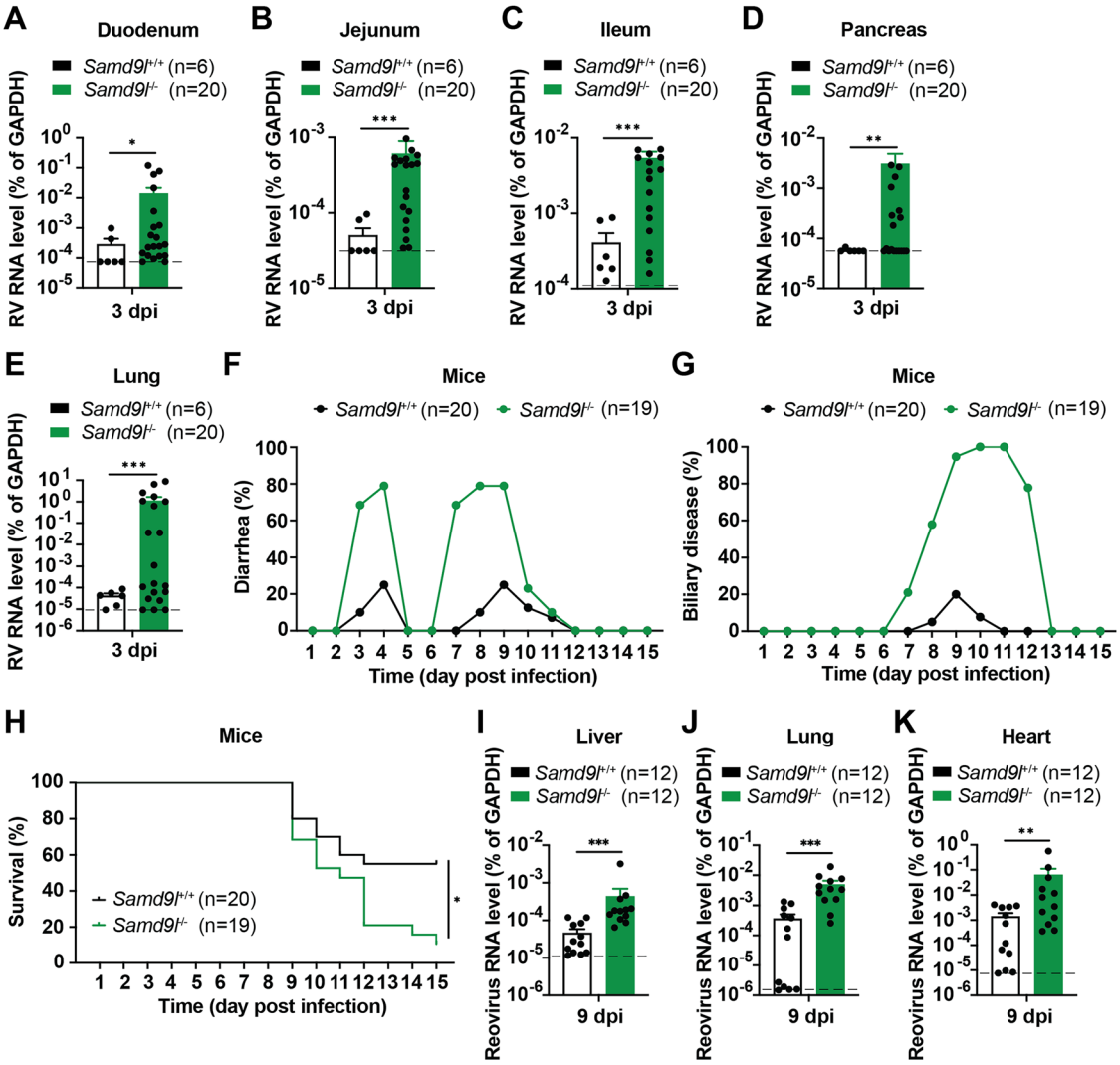

Fig. 7 | *Samd9l*$^{-/-}$ mice are more susceptible to dsRNA virus infections. A–E Five-day-old *Samd9l*$^{+/+}$ and *Samd9l*$^{-/-}$ neonatal mice orally infected with simian RV (2.4×10^7 FFU per mouse). RNA extracted from duodenum (**A**), jejunum (**B**), ileum (**C**), pancreas (**D**) and lung (**E**) collected at 3 dpi, and RV NSP5 mRNA levels measured by qRT-PCR. Dotted lines: limits of detection. **F–H** Three-day-old *Samd9l*$^{+/+}$ and *Samd9l*$^{-/-}$ neonatal mice intraperitoneally injected with reovirus (1×10^4 PFU per mouse) and the percentages of diarrhea development (**F**), biliary disease (**G**), or survival (**H**) recorded from days 1 to 15 post-infection. **I–K** Three-day-old *Samd9l*$^{+/+}$ and *Samd9l*$^{-/-}$ neonatal mice intraperitoneally injected with reovirus (1×10^4 PFU per mouse). RNA extracted from liver (**I**), lung (**J**) and heart (**K**) collected at 9 dpi, and reovirus mRNA levels measured by qRT-PCR. Dotted lines: limits of detection. For all figures, experiments were repeated at least three times. Individual points in (**A–E** and **I–K**) represent individual mouse. Data are represented as mean ± SEM. Statistical significance calculated by unpaired two-tailed Student's *t*-test (**A–E** and **I–K**), or log-rank test (**L**): $^*P < 0.05$, $^{**}P < 0.01$, $^{***}P < 0.001$. Source data are provided as a Source Data file. Detailed *P*-values are provided in the Source Data file.

despite the relative lack of sequence identity, SAMD9 and SAMD9L from various species could be structurally similar and thus allow similar functions, as predicted by Alphafold-2. The nucleic acid-binding footprint within SAMD9 is between 20 to 40 bp and 20 to 42 bp for dsDNA and dsRNA, respectively (Fig. 3D, F). Structural analysis of SAMD9, alone and in complex with dsDNA or dsRNA, should be informative in the determination of exact domains of SAMD9 critical for nucleic acid binding because both AlbA and OB seem dispensable (Fig. 4E–G and Supplementary Fig. 11). We also considered the possibility that IFN induction by SAMD9/9L is not mediated by adaptor proteins since protein-protein interactions tend to be less conserved. An analysis of SAMD9 phylogeny predicts the presence of functional SAMD9 homologs in bacteria[24]. This is reminiscent of cGAS, which displays anti-phage activities in many bacterial species[70,71]. Also analogous to the cGAS-STING signaling[72,73], it will be of interest to test whether SAMD9 senses retrovirus infections, although it will be complicated by at least two issues: whether SAMD9 binds DNA/RNA hybrid and if SAMD9 sensing is important in immune cells. Other ligands worth investigation include various vaccine adjuvants and self-derived dsDNA and dsRNA molecules arising in the context of tumor progression and autoimmune diseases.

Methods

Cell culture, plasmids, and viruses

Sf9 cells (ATCC #CRL-1711) were cultured in Grace's Insect Medium (Gibco #11605-094) supplemented with 10% heat-inactivated insect cell culture tested fetal bovine serum (Sigma #F4135). High five cells (Gibco #B85502) were grown in Express Five serum-free medium (Gibco #10486025) supplemented with 1× L-glutamine (Gibco #25030081). A549 cells (ATCC #CCL-185), Hela (ATCC #CCL-2), HEK293 (ATCC #CRL-1573), and HEK293T cells (ATCC #CRL-3216) were cultured in advanced DMEM (Gibco #12491050) supplemented with 10% heat-inactivated selected grade fetal bovine serum (Avantor Seradigm #89510-186) and 1× Penicillin-Streptomycin-Glutamine (Gibco

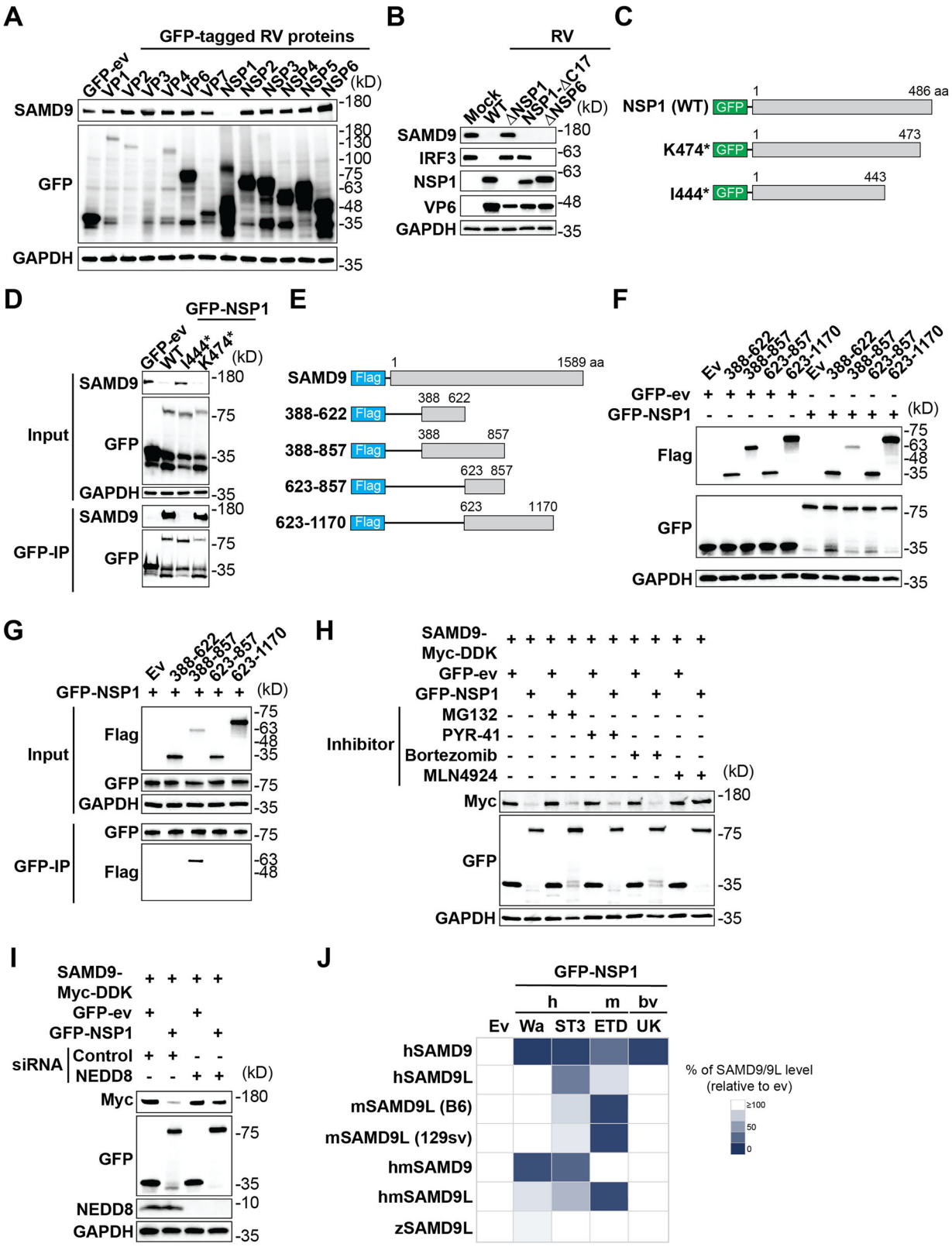

#10378016). *MAVS* KO A549 cells were kindly gifted by Yize Li (Arizona State University, AZ, USA). HT-29 cells (ATCC #HTB38) were grown in advanced DMEM F12 (Gibco #12634010) supplemented with 10% heat-inactivated fetal bovine serum, 1× Penicillin-Streptomycin-Glutamine, 10 mM HEPES (Gibco #15630106), 1× Non-Essential Amino Acids Solution (Gibco #11140050), and 1 mM sodium pyruvate (Gibco #11360070). MA104 cells (ATCC #CRL-2378.1) were cultured in Medium 199 (Gibco #11150059) supplemented with 10% heat-inactivated fetal bovine serum and 1× Penicillin-Streptomycin-Glutamine. Primary human cardiomyocytes (PromoCell #C-12810) were cultured in Myocyte growth medium (PromoCell #C-22070). Primary human dermal fibroblasts (ATCC #PCS-201-012) were grown in DMEM (Gibco #11960-044) supplemented with 10% heat-inactivated fetal bovine serum, 1× Penicillin-Streptomycin-Glutamine, 10 mM

Fig. 8 | Rotavirus NSP1 is a viral antagonist of SAMD9. A HEK293 cells transfected with GFP-ev, or GFP-tagged RV-encoded proteins (VP1-VP4, VP6, VP7, and NSP1-NSP6) for 48 h and cell lysates harvested for SDS-PAGE electrophoresis with indicated antibodies. **B** MA104 cells infected by indicated recombinant simian RV SA11 (MOI = 3) for 8 h and cell lysates harvested for SDS-PAGE electrophoresis with indicated antibodies. **C** Schematic representation of N-terminally GFP-tagged WT and truncated RV NSP1 constructs. **D** Immunoblotting analysis of anti-GFP antibody immunoprecipitates of cell lysates from HEK293 cells transfected with GFP-tagged WT or truncated NSP1s. **E** Schematic representation of N-terminally 3 × Flag-tagged WT and truncated SAMD9 constructs. **F** HEK293 cells co-transfected with Flag-tagged SAMD9 mutants and GFP-ev or GFP-NSP1 for 48 h and cell lysates harvested for SDS-PAGE electrophoresis with indicated antibodies. **G** Immunoblotting analysis of anti-GFP antibody immunoprecipitates of cell lysates from HEK293 cells co-transfected with GFP-tagged NSP1 and Flag-tagged SAMD9 mutants. **H** HEK293 cells co-transfected with SAMD9-Myc-DDK and GFP-ev or GFP-NSP1 for 36 h, treated with MG132 (10 μM), PYR-41 (50 μM), bortezomib (10 μM), or MLN4924 (10 μM) for another 12 h, and cells lysates harvested for SDS-PAGE electrophoresis with indicated antibodies. **I** HEK293 cells transfected with control or NEDD8-specific siRNA for 48 h, then co-transfected with SAMD9-Myc-DDK and GFP-ev or GFP-NSP1 for another 36 h, and cell lysates harvested for SDS-PAGE electrophoresis with indicated antibodies. **J** Relative abundance of SAMD9 and SAMD9L protein levels from indicated species in *SAMD9* KO HEK293 co-transfected with indicated SAMD9 or SAMD9L and NSP1s derived from different RV strains. Bv bovine. Darker colors indicate a higher level of SAMD9/9L inhibition by NSP1. For all figures, experiments were repeated at least three times.

HEPES, 1× Non-Essential Amino Acids Solution, 1 mM sodium pyruvate, and 5.5 μM 2-Mercaptoethanol. Human monocyte THP-1 cells (ATCC #TIB-202) were cultured in RPMI 1640 medium (Gibco #11875093) supplemented with 10% heat-inactivated fetal bovine serum and 1× Penicillin-Streptomycin-Glutamine. BHK-T7 cells were kindly gifted by Ursula Buchholz (Laboratory of Infectious Diseases, NIAID, NIH, USA). Cells were cultured in advanced DMEM supplemented with 10% heat-inactivated selected grade fetal bovine serum, 1× Penicillin-Streptomycin-Glutamine, and 0.3 mg/ml G418 (Gibco #10131035). MA104-N*V cells were grown in Medium 199 supplemented with 10% heat-inactivated fetal bovine serum, 1× Penicillin-Streptomycin-Glutamine, and 10 μg/ml of puromycin (Selleckchem #S7417) and blasticidin (Selleckchem #S7419) as previously reported[60]. Primary human hepatocytes (Lonza #HUCPG) were cultured in hepatocyte culture medium (Lonza #CC-3198).

PUC19 (Addgene #50005), pFastBac-M2 (Addgene #135583), pCMV6-Entry (Origene #PS100001), human SAMD9-Myc-DDK (Origene #RC219076), human SAMD9-pLenti-C-Myc-DDK-P2A-Puro (Origene #RC219076L3), human SAMD9-pLenti-C-mGFP (Origene #RC219076L2), human SAMD9L-Myc-DDK (Origene #RC214427), mouse SAMD9L-Myc-DDK (Origene #MR216450), IRF1-Myc-DDK (Origene #RC203500) were obtained from commercial vendors as indicated above. The OB-fold domain (1339–1589 amino acids)-deletion (ΔOB) human SAMD9 constructs were generated by QuikChange II site-directed mutagenesis kit (Agilent Technology #200524), based on human SAMD9-pLenti-C-mGFP and SAMD9-pLenti-C-Myc-DDK-P2A-Puro vectors. The AlbA domain (195–385 amino acids)-deletion (ΔAlbA), AlbA and OB-fold domains double deletion (ΔAlbA+OB) human SAMD9 plasmids were generated as mentioned above based on human SAMD9-Lenti-C-mGFP vector. The full-length human SAMD9L (CL20c-MIG-DEST-SAMD9L) and SAMD9L-ΔOB (CL20c-MIG-DEST-SAMD9L-ΔOB) plasmids were previously published[74] and kind gifts from Dr. Jeffery M. Klco at St. Jude Children's Research Hospital. To clone SAMD9 and SAMD9L from golden hamster and zebrafish, total RNA from lung tissue of golden hamster and embryos of zebrafish, respectively, was extracted by TRIzol reagent (Thermo Fisher Scientific #15596026) and reverse-transcribed to cDNA. Full-length SAMD9 and SAMD9L fused with 5′ AsiSI (New England Biolabs #R0630) and 3′ NotI (New England Biolabs #R0189) restriction enzyme sites were amplified using Phusion Hot Start II DNA Polymerase (Thermo Fisher Scientific #F549). The pCMV6-Entry vector, SAMD9, and SAMD9L fragments were digested by AsiSI and NotI for 3 h at 37 °C. The digested fragments were gel-purified and ligated with pCMV6-Entry using T4 DNA Ligase (New England Biolabs #M0202). To generate 129S6/SvEv mSamd9l construct, V169 and I459 of C57Bl/6J mSamd9l were mutated to I169 and V459, respectively, using QuikChange II site-directed mutagenesis kit based on the C57Bl/6J mSamd9l-Myc-DDK plasmid. The pG-LAP6 empty vector (ev) and pG-LAP6-RRV-NSP1/SA11-5S-NSP1/Wa-NSP1/ST3-NSP1/UK-NSP1/ETD-NSP1 plasmids were previously reported[75]. To insert RRV VP1-VP4, VP6, V7, and NSP2-6 into pG-LAP6-ev, the 11 corresponding genes were cloned from T7-RRV genome plasmids[60], then introduced into pENTR221 vector using BP reaction (Invitrogen #11789021), and transferred to the pG-LAP6 destination vector by LR reaction (Invitrogen #11791020). pG-LAP6-Wa-NSP1-M83*/N176*/C324*/A475* plasmids were previously published[75]. To construct the pG-LAP6-Wa-NSP1-I444*/K474* mutants, amino acids position 444 or 474 of Wa-NSP1 were mutated to premature stop codons using QuikChange II site-directed mutagenesis kit based on pG-LAP6-Wa-NSP1 plasmid. The pTriEX-4 empty vector with a N-terminal 3x Flag (ev), SAMD9-1-385 aa overexpression plasmid (1–385 aa), and SAMD9-1170-1589 aa overexpression plasmid (1170–1589 aa) were previously published[52]. To generate more SAMD9 overexpression mutants in pTriEX-4-3xFlag, SAMD9-388-1170/388-622/388-857/623-857/623-1170 aa fragments were amplified using Phusion Hot Start II DNA Polymerase, and cloned into the pTriEx-4-3xFlag by Gibson Assembly Cloning Kit (New England BioLabs #E5510). The generated clones were verified by Sanger sequencing.

Cells (1×10^5) were seeded in 24-well plates for 3 days. For human (WI61, G9P[8]) and animal rotavirus (RRV, G3P[3] and UK, G6P[5]) infections, cells were washed by serum-free medium twice and then infected at a multiplicity of infection (MOI) of 0.1 for 1 h at 37 °C. The inoculum was washed three times with serum-free medium and fresh serum-free medium supplemented with 0.02 μg/ml of trypsin (Sigma-Aldrich #T0303) was added to the infected cells for 24 h at 37 °C. For reovirus (T1L strain), influenza A virus (H3N2 A/Victoria/261/2011), vesicular stomatitis virus (Indiana strain, a kind gift from Dr. Jack Rose at Yale University), chikungunya virus (strain 181/25), Zika virus (strain P6-740), human astrovirus (Yuc8 strain, a kind gift from Dr. Carlos Arias at UNAM), adenovirus (serotype 5), modified vaccinia virus (Ankara strain, ATCC VR-1508), monkeypox virus (hMPXV/USA/MA001/2022 strain), and herpes simplex virus type 1 infection, cells were inoculated with indicated viruses at an MOI of 0.1 for 1 h at 37 °C. After the inoculum was aspirated, cells were washed with complete medium three times, then new complete medium was added to the infected cells for 24 h at 37 °C.

Immunoprecipitation and mass spectrometry

HT-29 cells (2×10^6) were cultured in 10-cm cell culture-treated dishes for 24 h. Cells were washed three times with ice-cold PBS (Gibco #10010023), harvested using cell scrapers, and pelleted by centrifugation at 500×*g* for 5 min at 4 °C. The cell pellets were lysed in 1 ml NP-40 lysis buffer containing 1× protease inhibitor cocktail (Thermo Fisher Scientific #87786) for 30 min on ice. Cell lysates were clarified by centrifuging at 13,000 rpm for 10 min at 4 °C. The clarified cell lysates were then incubated with 100 ng biotinylated 48,502-bp dsDNA (LUMICKS #00001), 20,452-bp ssDNA (LUMICKS #00014), LPS-EB (InvivoGen #tlrl-lpsbiot), or dsRNA analog HMW poly(I:C) (InvivoGen #tlrl-picb) for 2 h at 4 °C. Meanwhile, Dynabeads M-280 Streptavidin (Invitrogen #11205D) were blocked in 5% BSA buffer for 2 h at 4 °C. Following this, the mixtures were incubated with blocked streptavidin beads overnight at 4 °C. Subsequently, the streptavidin beads were washed five times with PBS and boiled in 20 μl 2× Laemmli Sample

Buffer for 5 min at 95 °C. The boiled samples were loaded into 4–15% Mini-PROTEAN TGX Precast Gel (Bio-Rad #4561083EDU) and run at 100 V for 10 min. The bands were excised from the gel and submitted for Mass Spectrometry analysis at the McDonnell Genome Institute, Washington University School of Medicine. The mass spectrometry samples were analyzed using Mascot (Matrix Science, London, UK; version 2.8.3). Mascot was set up to search the uniprot-Human-SP_Version2021-04_20220111_20220111 database assuming the digestion enzyme trypsin. Mascot was searched with a fragment ion mass tolerance of 0.60 Da.

RNA sequencing

A549 cells (4×10^5) were seeded in 6-well plates and cultured overnight before transfection. Cells were transfected with pCMV6-entry or SAMD9-Myc-DDK (2 μg) by Lipofectamine 3000 for 24 h. The total RNA was extracted by RNeasy Mini Kit (Qiagen #74104) and qualified by NanoDrop spectrophotometer (Thermo Fisher). Samples were prepared according to library kit manufacturer's protocol, indexed, pooled, and sequenced on an Illumina NovoSeq. Basecalls and demultiplexing were performed with Illumina's bcl2fastq software and a custom Python demultiplexing program with a maximum of one mismatch in the indexing read. RNA-seq reads were then aligned to the Ensembl release 76 primary assembly with STAR version 2.5.1a[76]. Gene counts were derived from the number of uniquely aligned unambiguous reads by Subread:featureCount version 1.4.6-p5[77]. Isoform expression of known Ensembl transcripts were estimated with Salmon version 0.8.2[78]. Sequencing performance was assessed for the total number of aligned reads, total number of uniquely aligned reads, and features detected. The ribosomal fraction, known junction saturation, and read distribution over known gene models were quantified with RSeQC version 2.6.2[79]. To find the most critical genes, the raw counts were variance stabilized with the R/Bioconductor package DESeq2[80] and were then analyzed via weighted gene correlation network analysis with the R/Bioconductor package WGCNA[81].

Quantitative reverse transcription-real-time polymerase chain reaction

RNA samples were extracted as described above. RNA was reverse-transcribed by High-Capacity cDNA Reverse Transcription Kit (Thermo Fisher Scientific #4368814) and the quantitative PCR was performed by SYBR Green qPCR ReadyMix (Sigma-Aldrich #KCQS00) or Taqman assays (Applied Biosystems #4444557)[82]. The primers used in this study were: GAPDH forward primer: 5′-GGAGCGAGATCCCTC CAAAAT-3′, reverse primer: 5′-GGCTGTTGTCATACTTCTCATGG-3′; IFNB forward primer: 5′-ATGACCAACAAGT GTCTCCTCC-3′, reverse primer: 5′-GGAATCCAAGCAA GTTGTAGCTC-3′; IFNL3 forward primer: 5′-TAAGAGGGCCAAAGATGCCTT-3′, reverse primer: 5′-CTGGTCCAA GACATCCCCC-3′; CCL5 forward primer: 5′-CCAGCAGTCGTC TTTGTCAC-3′, reverse primer: 5′-CTCTGGGTTGGCACACACTT-3′; CXCL10 forward primer: 5′-GTGGCATTC AAGGAGTACCTC-3′, reverse primer: 5′-TGATGGCCTTCGAT TCTGGATT-3′; MX1 forward primer: 5′-GTGGCTGAGAACAACCTGTG-3′, reverse primer: 5′-GGCATCTGG TCACGATCCC-3′; RV NSP5 forward primer: 5′-CTGCTTCAAA CGATC-CACTCAC -3′, reverse primer, 5′-TGAATCCATAGACACGCC-3′, and probe, 5′-CY5/TCAAATGCAG TTAAGACAAATGCAGACGCT/IABRQSP-3′; Reovirus T1F forward primer: 5′-GCATCC ATTGTAAATGAC-GAGTCTG-3′; reverse primer: 5′-CTTGAGATTAG CTCTAGCATCTTC TG-3′; IAV-A1 forward primer: 5′-AAGACCAATCCTGTCACCTCTG A-3′, reverse primer: 5′-CAAAGCGTCTACGCTGCAGTCC-3′; VSV N forward primer: 5′-GATAGTACCGGAG GATTGACGACTA-3′, reverse primer: 5′-TCAAACCATCCGAGCC ATTC-3′; CHIKV forward primer: 5′-AAGCTCCGCGTCCTTTACCAAG-3′, reverse primer: 5′-CCAAATTGT CCTGGTCTTCCT-3′; ZIKV forward primer: 5′-TTGGTCATGATACTGC TGATTGC-3′, reverse primer: 5′-CCTTCCACAAAGTCCCTATTGC-3′; HAstV forward primer: 5′-CAGGCTTTACCCACAT-3′, reverse primer: 5′-TACAGACATGTGCATGAATG G-3′; AdV forward primer: 5′-GACATGAC TTTCGAGGTCGATCCCATGG-3′, reverse primer: 5′-CCGGCTGAGAAGG GTGTGCGCAGGTA-3′; MVA forward primer: 5′-GGCAA TGGATTCAGG GATATAC-3′, reverse primer: 5′-ATTTATGAATAATCCGCCAGTTAC-3′. HSV-1 ICP27 forward primer: 5′-TTTCTCCAGTGCTACCTGAAGG-3′, reverse primer: 5′-TCAACTCGCAGACACGACTCG-3′. Mouse Gapdh forward primer: 5′-TCTGGAAAGCTGTGCCGTG-3′, reverse primer: 5′-C CAGTGAGCTTCCCGTTCAG-3′; mouse Ifnl3 forward primer: 5′-AGCTG CAGGCCTTCAA AAAG-3′, reverse primer: 5′-TGGGAGTGAATGTGGC TCAG-3′. Monkeypox virus was measured by a Hemagglutinin Gene-Specific Quantitative PCR Assay Detection Kit (BEI #NR-9351). Mouse Samd9l Taqman primers were ordered commercially (Thermo Fisher Scientific #Mm00612478_s1). Human SAMD9 Taqman primers were ordered commercially (Thermo Fisher Scientific #Hs00539471_s1).

Solid-phase enzyme-linked immunoabsorbent assay

Secreted IFN-λ3 and CCL5 levels were tested with human IL-29/IL-28B (IFN-lambda 1/3) DuoSet ELISA kit (R&D Systems #DY1598B05) and human CCL5/RANTES DuoSet ELISA kit (R&D Systems #DY27805) according to the manufacturer's protocol.

SDS-PAGE immunoblotting

For Coomassie, recombinant His-SAMD9 was mixed with 2× Laemmli Sample Buffer (Bio-Rad #1610737) and boiled for 5 min at 95 °C. The samples were resolved in the 4–15% Mini-PROTEAN TGX Precast Gel with 1× Tris/Glycine/SDS buffer (Bio-Rad #1610772). Gels were stained by Coomassie Brilliant Blue R-250 staining solution (Bio-Rad #1610436), then destained with 20% ethanol (v/v) and 10% acetic acid (v/v).

For immunoblotting, cell lysates were prepared by lysing cells in RIPA buffer (Thermo Fisher Scientific #J63306-AK) with 1× protease inhibitor cocktail for 10 min on ice. Cell lysates were clarified by centrifuging at 13,000 rpm for 10 min at 4 °C, and the supernatant was mixed with 2× Laemmli Sample Buffer and boiled for 5 min at 95 °C. The samples were resolved in 4–15% Mini-PROTEAN TGX Precast Gel with 1× Tris/Glycine/SDS buffer and the rest of the steps were the same as Native-PAGE immunoblotting described above. The antibodies used here were as follows: SAMD9 (Sigma-Aldrich #HPA021319, 1:5000), RIG-I (Cell signaling #3743, 1:1000), MDA5 (Cell signaling #5321, 1:1000), MAVS (Cell signaling #24930, 1:1000), STING (Cell signaling #13647, 1:1000), TBK1 (Cell signaling #3504, 1:1000), IRF3 (Cell signaling #4302, 1:1000), phospho-IRF3 (Cell signaling #29047, 1:1000), VP6 (Santa Cruz #sc-101363, 1:1000), GAPDH (Cell signaling #2118, 1:5000), EEA1 (Cell signaling #3288, 1:1000), Niemann Pick C1 (NPC1) (Abcam #ab134113, 1:1000), Rab11 (Cell signaling #3539, 1:1000), Calnexin (Abcam #ab22595, 1:1000), Golgin-97 (Cell signaling #13192, 1:1000), Cytochrome c (Abcam #ab13575, 1:1000), α-Tubulin (Cell signaling #2144, 1:1000), Histone H3 (Cell signaling #14269, 1:1000), SAMD9 (Invitrogen #PA5-54379, 1:1000), SAMD9L (Proteintech #25173-1-AP, 1:1000), GFP (Santa Cruz #sc-9996, 1:500), Flag (Sigma-Aldrich #F1804, 1:5000), anti-rabbit IgG HRP antibody (Cell signaling #7074, 1:5000), anti-mouse IgG HRP antibody (Cell signaling #7076, 1:5000). The membrane was imaged with ChemiDoc MP Imaging System.

Lentiviral transduction

Lentiviruses encoding Cas9 and single-guide RNA (sgRNA) against *SAMD9*, *STING*, *TBK1* and *IRF3* were harvested from the medium of HEK293T cells transfected with lenti-CRISPR_v2 vector expresses Cas9 and indicated sgRNA, VSV-G, and Gag-Pol. The pooled knockout A549 cells were generated by transduction with lentiviruses obtained above for 48 h, then the cells were selected by puromycin (2 μg/ml) for 2 weeks. To isolate single clonal *TBK1* KO A549 cells, the pooled *TBK1* KO A549 cells were subcloned using limiting dilutions in 96-well plates. For pooled knockout primary human cardiomyocytes, primary human

dermal fibroblasts, and human monocyte THP-1 cells, cells were infected with lentiviruses encoding Cas9 and sgRNA against SAMD9 for 48 h and then placed under puromycin selection (2 μg/ml) for 3 weeks.

To generate SAMD9 add-back *SAMD9* KO HT-29 cells, lentiviruses encoding SAMD9-Myc-DDK, SAMD9-mGFP or SAMD9-ΔOB-mGFP were harvested as described above. The SAMD9 KO HT-29 cells were transduced with lentiviruses bearing SAMD9-Myc-DDK for 48 h, then the cells were selected by puromycin (2 μg/ml) for 2 weeks to generate pooled rescue cells. To generate single clone SAMD9-mGFP or pooled clone SAMD9-ΔAlbA-mGFP, SAMD9-ΔOB-mGFP, and SAMD9-ΔAlbA +OB-mGFP rescue cells, *SAMD9* KO HT-29 cells were transduced with lentiviruses encoding SAMD9-mGFP, SAMD9-ΔAlbA-mGFP, SAMD9-ΔOB-mGFP, and SAMD9-ΔAlbA+OB-mGFP for 48 h, then the GFP-positive single cells were sorted into 96-well plates or 5-ml flow cytometry tubes by BD FacsAriaII Cell Sorters at the Flow Cytometry & Fluorescence Activated Cell Sorting Core at Washington University.

Immunofluorescence microscopy

To detect the localization of IRF3 by SAMD9 overexpression, A549 cells (1×10^5) were seeded on top of the microscope cover glasses (Thorlabs #CG15NH1) in 24-well plates, and transfected with Ev or SAMD9-Myc-DDK for 24 h, then fixed with 4% paraformaldehyde at RT for 10 min, and stained with different primary antibodies at RT for 1 h, followed by stained with different secondary antibodies at RT for 1 h[83].

To determine SAMD9 staining by regular fluorescent microscopy, A549 cells (1×10^5) were grown in 24-well plates. The immunofluorescence staining was done as described above. Stained cells were imaged with REVOLVE4 microscope (ECHO) with a 10× objective.

To observe the distribution of SAMD9 by super-resolution microscopy, WT or *SAMD9* KO HT-29 cells (3×10^4) were seeded on top of the microscope cover glasses (Thorlabs #CG15NH1) in 24-well plates. The immunofluorescence staining was done as described above. The images were taken by the Nikon n-SIM Structured Illumination microscope at a 100× oil immersion high NA lens at the Center for Cellular Imaging at Washington University.

To detect SAMD9 colocalization with dsRNA or dsDNA, A549 (3×10^4) cells were seeded on top of the microscope cover glasses in 24-well plates. The cells were either infected by rhesus RV RRV strain at an MOI of 300, or transfected with poly(dA:dT)/LyoVec or poly(I:C)-LMW/LyoVec at a concentration of 10 μg/ml for 8 h. Cells were fixed, stained as described above, and imaged with a Zeiss LSM880 Confocal Microscope at the Molecular Microbiology imaging core facility at Washington University. Colocalization was analyzed by Volocity v6.3 (PerkinElmer).

The antibodies or fluorescent dyes used in this study were: SAMD9 (Sigma-Aldrich #HPA021319, 1;5000), SAMD9 (Invitrogen #PA5-54379, 1:5000), SAMD9 (Abcam #ab180575, 1:5000), dsDNA (Santa Cruz #sc-58749, 1:200), dsRNA-9D5 (Absolute antibody #Ab00458-23, 1:200), α-tubulin (Sigma-Aldrich #T7451, 1:5000), MUC2 (Alexa Fluor 488, Santa Cruz #sc-515032, 1:250), phalloidin (Alexa Fluor 647, Thermo Fisher #A22287, 1:250), 4′,6-diamidino-2-phenylindole (DAPI) (Invitrogen #D3571, 1:1000), goat anti-Rabbit IgG (H + L) Cross-Adsorbed Secondary Antibody-Alexa Fluor 488 (Invitrogen #A-11008, 1:250), donkey anti-Mouse IgG (H + L) Highly Cross-Adsorbed Secondary Antibody-Alexa Fluor 594 (Invitrogen #A-21203, 1:250).

CRISPR/Cas9 single clone knockout

To generate single clonal knockout cells, HT-29 cells were transfected with PX458 vector expresses Cas9 and sgRNA against *SAMD9*, *RIG-I*, *MDA5*, *MAVS*[37], and *STING* for 48 h. HEK293 and A549 cells were transfected with PX458 with Cas9 and *SAMD9* sgRNA for 48 h. GFP-positive single cells were sorted into 96-well plates by BD FacsAriaII Cell Sorters at the Flow Cytometry & Fluorescence Activated Cell Sorting Core at Washington University. Single clonal knockout HT-29 cells, HEK293 or A549 cells were screened based on western blot and Sanger sequencing. To generate *RIG-I MDA5* double knockout HT-29 cells, *RIG-I* KO HT-29 cells were transfected with PX458 vector bearing Cas9 and sgRNA against *MDA5* for 48 h, and the single clonal cells were selected as described above. CRISPR sgRNA sequences used in this study were: SAMD9: CGAGAAGTCTTGCAACCAAT; STING: GTGACCC CTGGGACACGGGA; RIG-I: GGCATCCCCAACACCAACCG; MDA5: GGT GAAAATGTACATCCAGG. The sequencing primers used for single clonal knockout HT-29 cells were: SAMD9 forward primer: 5′-GCAGG AGAAACCTAGTAGC-3′, reverse primer: 5′- GTGAACAAGTCTTTCC AG TC-3′; RIG-I forward primer: 5′-GCATTATGTGCC TCCATG-3′, reverse primer: 5′-GG GATGAGAGCTCAGTTAGAG-3′; MDA5 forward primer: 5′-CTGCTTCTCTAAGTGGGC AG-3′, reverse primer: 5′-TGAGCTCAGG GTTCA TGTAG-3′; STING forward primer: 5′-GAAAGGGGAACTGGGA G-3′, reverse primer: 5′-AGTCACCT GGAGTGGATGT-3′.

Cytosolic dsDNA, ssDNA, and dsRNA stimulation

Cells were seeded in 24-well plates at a density of 1×10^5 cells/ml, cultured for 48 h, and then incubated with poly(dA:dT)/LyoVec (Invivogen #tlrl-patc) or poly(I:C)-LMW/LyoVec (Invivogen #tlrl-picwlv) at a concentration of 1 μg/ml for 24 h. For herring testes DNA (HT-DNA) (Sigma-Aldrich #D6898) and ssRNA polyU (Invivogen #tlrl-sspu) stimulation, cells were plated as above, then 0.5 μg of HT-DNA, 5 μg of ssRNA polyU, or 5 μg of ODN2216 was mixed with 3.125 μg, 31.25 μg, or 31.25 μg of LyoVec (Invivogen #lyec-1), respectively, in a 50 μl volume for 30 min at room temperature, then the complexes were mixed with 450 μl complete medium and added on to the cells for 24 h.

SAMD9 expression and purification

N-terminal 10 × His-tag and 3 C protease cleave site fused SAMD9 (referred to as His-SAMD9) was cloned based on human SAMD9-Myc-DDK plasmid, and then inserted into a pFastBac-M2 vector. The recombinant pFastBac-M2 vector was transformed into DH5α competent cells and Maxi-prepped to generate the Bacmid. The Bacmid was transfected into sf9 cells to produce baculovirus stock (P1), and the new sf9 cells were infected by the P1 virus to generate P2 virus. 7 liters of High five cells were infected by P2 virus (MOI = 1) for 2 days at 27 °C, then the cells were harvested and resuspended in Buffer A (20 mM PB, 500 mM NaCl, 10% Glycerol, 0.1% Triton X-100, 1 × protease inhibitor cocktail, pH 7.0). After sonication, the cell lysates were clarified by ultracentrifugation at 100,000×*g* for 1 h at 4 °C. The supernatant with an addition of 10 mM imidazole was loaded onto 4 ml bed volume Ni-NTA resin (Roche #5893682001), then washed with 100 ml Buffer A with 20 mM imidazole. The SAMD9 was finally eluted by 20 ml Buffer A with 500 mM imidazole. The eluted SAMD9 was further purified by HiLoad Superdex 200 pg preparative SEC columns (Cytiva #28989335), and buffer exchanged to Buffer B (20 mM PB, 300 mM NaCl, 10% Glycerol, pH 7.0). All the purification steps were done at 4 °C. The final products were aliquoted and flash frozen in liquid nitrogen, then stored in −80 °C for future experiments.

His-MBP-tagged human SAMD9, SAMD9-ΔOB, and SAMD9-ΔAlbA+OB proteins were purified using amylose resin according to the manufacturer's instructions. After the elution from the affinity purification, both of the samples were concentrated and subjected to size-exclusion chromatography with a buffer composition of 20 mM HEPES, 150 mM NaCl and 1 mM DTT. The non-tagged SAMD9-ΔAlbA+OB proteins were generated by removing His-MBP-tag from tagged SAMD9-ΔAlbA+OB proteins using TEV protease (NEB #P8112S).

Oligonucleotides for dsDNA, ssDNA, and dsRNA

To generate dsDNA fragments of different lengths, including 80, 160, 320, 640, and 1280 bp, we designed a set of unique primers randomly based on NCBI Primer BLAST and pUC19. The dsDNA products were amplified by Phusion Hot Start II DNA Polymerase (Thermo Fisher Scientific #F549S) and purified by agarose gel using QIAquick Gel Extraction Kit (QIAGEN #28706). The 15, 20-bp dsDNA, and 80-bp ssDNA were synthesized randomly or according to the sense strand of 80-bp dsDNA. The primers or sequence used in this study were: 80-bp dsDNA forward primer: 5′-CGCCTACATACCTCGCTCTG-3′, reverse primer: 5′-GTCCAACCCGGTAAGACAC G-3′; 160-bp dsDNA forward primer: 5′-GCGTAATAGCGAAGAGGCCC-3′, reverse primer: 5′-CTATGC GGCATCAGAGCAGAT-3′; 320-bp dsDNA forward primer: 5′-CGGC ATCCGCTTACAGACAA-3′, reverse primer: 5′-CCGTGTCGCCCTTATT CCC-3′; 640-bp dsDNA forward primer: 5′-CCTCTGACTTGAGCGTC GATT-3′, reverse primer: 5′-CGGG CCTCTTCGCTATTACG-3′; 1280-bp dsDNA forward primer: 5′-GCACGAGTGGGTTAC ATCGA-3′, reverse primer: 5′-GTGTAGGTCGTTCGCTCCAAG-3′; 15-bp dsDNA: 5′-GATAAG GACTCGTAT-3′; 20-bp dsDNA: 5′-GATAAGGACTCGTATGTACC-3′. 80-bp ssDNA: 5′-CG CCTACATACCTCGCTCTGCTAATCCTGTTACCAG TGGCTGCTGCCAG TGGCGATAAGTCGTGTCTTACCGGGTTGGAC-3′. 16, 20, 42, 112, 162, and 512-bp dsRNA was used as previously described[84].

Electrophoretic mobility shift assay (EMSA)

For the circular dsDNA (pUC19 plasmid) EMSA assay, His-SAMD9 (1 μM) was mixed with pUC19 at a molar ratio of 0, 2:1, 4:1, and 8:1 in Buffer C (300 mM NaCl, 5 mM $MgCl_2$, 1 mM DTT, 10% Glycerol, pH 7.0). The mixtures were incubated at 30 °C for 1 h. For the linear dsDNA or ssDNA EMSA assays, His-SAMD9 (1 μM) was incubated with dsDNA fragments with the lengths of 15, 20, 40, 80, 160, 320, 640, and 1280 bp, poly(dA:dT) (Invivogen # tlrl-patn), or 80-bp ssDNA at a 200:1 molar ratio in Buffer C. The mixtures were incubated at 30 °C for 1 h. For the dsRNA or ssRNA EMSA assays, His-SAMD9 (1 μM) was incubated with dsRNA fragments with the lengths of 16, 20, 42, 112, 162, and 512 bp, LMW or HMW-poly(I:C) (Invivogen #tlrl-picwlv or #tlrl-piclv), RV dsRNA (described below), ssRNA polyuridine (ssRNA polyU, Invivogen # tlrl-sspu) at a 200:1 molar ratio in Buffer C, in the presence of 200 U/ml RNase inhibitor (Thermo Fisher Scientific #N8080119), at 30 °C for 1 h. For titrating the binding affinity of His-SAMD9 with 512-bp dsRNA, His-SAMD9, ranging from 0, 25, 50, 100, 200, 400, and 800 nM, was incubated with 512-bp dsRNA (5 nM) at 30 °C for 1 h. To test the pUC19 binding with His-MBP-tagged SAMD9, His-MBP-SAMD9 (0.3 μM), His-MBP-SAMD9-ΔOB (0.3 μM), His-MBP-SAMD9-ΔAlbA+OB (0.3 μM), or non-tagged SAMD9-ΔAlbA+OB (0.3 μM) was mixed with pUC19 (0.00073 μM) as mentioned above. All experiments were performed on 0.8% agarose gel prepared in 0.5× tris-acetate-EDTA (TAE) buffer and run at 50 V at room temperature. Gels were stained with GelRed (Biotium #41003) and visualized by ChemiDoc MP Imaging System (Bio-Rad).

Native-PAGE electrophoresis

The native-PAGE electrophoresis was performed as described below[85]. For Coomassie, recombinant His-SAMD9 proteins were mixed with 2× Native Sample Buffer (Bio-Rad #1610738), loaded into 4–15% Mini-PROTEAN TGX Precast Gel (Bio-Rad #4561083EDU) directly, and run at 20 mA in cold room. The anode buffer contains 50 mM Tris and 384 mM glycine; the cathode buffer consists of 50 mM Tris, 384 mM glycine, and 1% sodium deoxycholate.

For detecting recombinant His-SAMD9 oligomerization, His-SAMD9 (1 μM) was incubated with pUC19 (0.125 μM) in Buffer C at 30 °C for 1 h and then the mixture was mixed with 2× Native Sample Buffer. The samples were loaded, resolved in precast gel as described above, and transferred to nitrocellulose membrane (Bio-Rad #1620215). The membrane was incubated with blocking buffer (5% bovine serum albumin (BSA) diluted in PBS supplemented with 0.1% Tween 20) for 1 h at room temperature. Then the membrane was incubated with an anti-SAMD9 rabbit monoclonal antibody (Sigma-Aldrich #HPA021319, 1:5000), followed by incubation with anti-rabbit IgG horseradish peroxidase-linked (HRP) antibodies (Cell Signaling #7074, 1:5000). The antigen-antibody complex was detected using Clarity Western ECL substrate (Bio-Rad #1705061) and ChemiDoc MP Imaging System according to the manufacturer's manuals.

For detecting intracellular SAMD9 oligomerization, A549 cells (5×10^5) in 6-well plates were infected with a recombinant simian rotavirus SA11 strain encoding GFP[86] at an MOI of 3 for 8 h. WT HT-29, SAMD9-mGFP or SAMD9-ΔOB-mGFP add-back *SAMD9* KO HT-29 cells (5×10^5) in 6-well plates were transfected with 10 μg/ml poly(dA:dT) or LMW poly(I:C) for 8 h. The infected or transfected cells were then lysed by NP-40 lysis buffer (Thermo Fisher Scientific #J60766-AK) for 30 min on ice and the cell lysates were clarified by ultracentrifugation at 13,000×*g* for 30 min at 4 °C, the supernatant was mixed with 2× Native Sample Buffer. The following steps were the same as described above. The primary antibodies used were: SAMD9 (Sigma-Aldrich #HPA021319, 1:5000), RIG-I (Cell Signaling #3743, 1:1000), and IRF3 (IBL #18781, 1:200).

Electron microscopy

His-SAMD9 (0.56 μM) was incubated with pUC19 (0.07 μM) in Buffer C at 30 °C for 1 h. The mixtures were fixed with 1% glutaraldehyde (Ted Pella Inc., Redding, CA) and allowed to absorb onto freshly glow-discharged formvar/carbon-coated copper grids for 10 min. Grids were then washed in distilled H_2O and stained with 1% aqueous uranyl acetate (Ted Pella Inc.) for 1 min. Excess liquid was gently wicked off and grids were allowed to air dry. Samples were viewed on a JEOL 1200EX transmission electron microscope (JEOL USA, Peabody, MA) equipped with an AMT 8-megapixel digital camera (Advanced Microscopy Techniques, Woburn, MA) at 100 kV.

Immunoprecipitation assays

WT HT-29, SAMD9-mGFP, SAMD9-ΔAlbA-mGFP, SAMD9-ΔOB-mGFP, or SAMD9-ΔAlbA+OB-mGFP add-back *SAMD9* KO HT-29 cells (1×10^7) in 10-cm cell culture dishes were washed with ice-cold PBS (Gibco #10010023) three times, harvested by cell scrapers, and pelleted by centrifugation at 500×*g* for 5 min at 4 °C. The cell pellets were lysed in 1 ml NP-40 lysis buffer as mentioned above. The cell lysates were incubated with or without 20 ng of biotinylated 48,502-bp dsDNA (LUMICKS #0020) for 2 h at 4 °C. In the meantime, the Dynabeads M-280 Streptavidin (Invitrogen #11205D) were blocked in 5% BSA buffer for 2 h at 4 °C. Then, the lysates-biotinylated dsDNA complexes were incubated with streptavidin beads at 4 °C for another 1 h. The streptavidin beads were washed with NP-40 lysis buffer 5 times by rotation for 5 min each time and boiled in 2× Laemmli Sample Buffer for 5 min at 95 °C.

To test cellular DNA immunoprecipitation by SAMD9, HEK293 cells (1×10^7) in 10-cm cell culture dishes were transfected with SAMD9-Myc-DDK or SAMD9-ΔOB-Myc-DDK (10 μg) for 24 h, then the cells were lysed as mentioned above. The cell lysates were incubated with anti-Flag M2 Magnetic Beads (Sigma-Aldrich #M8823) overnight at 4 °C, then the cell lysates-Magnetic Beads complexes were washed with NP-40 lysis buffer three times. The protein-DNA complexes were eluted from magnetic beads by incubating with 150 μl ChIP Elution Buffer (Cell Signaling #9003S) for 30 min at 65 °C with vortex every 3 min. The elution was resolved in 1% agarose gel, and the SDS-PAGE immunoblotting was conducted as mentioned above.

To determine the endogenous SAMD9 interacted with RV-NSP1, HEK293 cells (1×10^6) in 6-well plates were transfected with pG-LAP6-ev or pG-LAP6-RRV-NSP1 (2 μg) for 48 h, then the cell pellets were harvested as described above. The immunoprecipitation assay was performed using GFP-Trap Magnetic Agarose (ChromoTek #gtma)

according to the manufacturer's protocol. Briefly, the cells were lysed in 200 µl ice-cold Lysis Buffer supplemented with 1× protease inhibitor cocktail for 30 min on ice, mixing the lysates every 10 min, then the cell lysates were clarified by centrifuging at 17,000×*g* for 10 min at 4 °C. The supernatant was mixed with 300 µl ice-cold Dilution Buffer supplemented with 1× protease inhibitor cocktail, and incubated with 20 µl GFP-beads, which was blocked by 5% BSA Buffer for 2 h at room temperature, overnight at 4 °C. The lysates-GFP-beads complexes were washed with 500 µl Wash Buffer 3 times and boiled in 2× Laemmli Sample Buffer for 5 min at 95 °C. To characterize the key region of RV-NSP1 required for its interaction with SAMD9, HEK293 cells (1×10^6) in 6-well plates were transfected with pG-LAP6-ev or pG-LAP6-Wa-NSP1 (WT)/I444*/K474* (2 µg) for 48 h, then the immunoprecipitation assay was conducted as described above. To map the domain of SAMD9 interacted with RV-NSP1, HEK293 cells (1×10^6) in 6-well plates were co-transfected with pG-LAP6-Wa-NSP1 and pTriEX-4-3Flag-ev/SAMD9-1-385/388-1170/1170-1589/388-622/388-857/623-857/623-1170 (2 µg) for 48 h, then the immunoprecipitation assay was conducted as described above.

Rotavirus genomic dsRNA extraction

MA104 cells were infected by rhesus rotavirus RRV strain at an MOI of 0.01 for 48 h, then the cells were frozen-thawed three times. The cell debris in the crude lysates was clarified by centrifugation at 3000×*g* for 1 h at 4 °C. After that, the supernatant was purified by 40% (w/v) sucrose cushion in SW44 centrifuge tube at 35,000 rpm for 3 h at 4 °C. Viral RNA was extracted from pelleted viral particles that were resuspended in TRIzol.

Subcellular fractionation

A549 cells (1×10^6) were seeded in 10-cm cell culture dishes. The subcellular fractionation protocol was modified based on previous publications[87,88]. For SAMD9 distribution at steady state, A549 cells were washed with ice-cold PBS for three times, then 2 ml of HEPES buffer (25 mM HEPES, 150 mM NaCl, 2 mM EGTA, 1 mM DTT, 1 mM Na_3VO_4, 1 mM PMSF) was used to scrape the cells from the dishes. Cells were passed through a 23G syringe 160 times to get a homogenate, and spun at 170 *g* for 10 min, to get the pellet (P170) and supernatant (S170). The P170 was further passed through the 23G syringe another 160 times, and centrifuged at 370×*g* for 15 min. The pellet (P370) was resuspended in 3 ml HEPES buffer and placed into a 5-ml SW55 ultracentrifuge tube, 1 ml of 2.1 M sucrose was carefully added to the bottom of the tube, then subjected to centrifugation at 175,000×*g* for 1 h, the pellet was collected as the nuclei component. To separate the membrane-associated organelles and cytosolic component, S170 was subjected to centrifugation at 8000×*g* for 15 min to generate P8000 and S8000. For SAMD9 localization in virus-infected cells, A549 cells were infected by a recombinant simian RV SA11-GFP at an MOI of 3 for 8 h. The following steps were as same as described above. All the centrifugation steps were done at 4 °C.

Focus forming unit assay

WT, *SAMD9* KO, SAMD9-Myc-DDK rescued, and SAMD9-mGFP rescued HT-29 cells were infected with RRV at an MOI of 0.1 for 24 h. Cell lysates were collected and subjected to three cycles of freeze-thawing, and then the cell debris was removed by spinning the cells at 1000×*g* for 10 min. The supernatant was harvested, and the viruses were activated by incubation with trypsin (5 µg/ml) for 20 min at 37 °C. Activated viruses were serially diluted 10-fold and incubated with fully confluent MA104 cells in 96-well plates for 12 h. After that, the cells were fixed with 10% formalin, and permeabilized by 1% Triton X-100, followed by incubation with VP6 antibody (Santa Cruz #sc-101363, 1:1000), and anti-mouse IgG HRP antibody (Cell signaling #7076, 1:5000). At last, the cells were stained by 3-amino-9-ethylcarbazole HRP substrate (Vector Laboratories #SK-4200) and stopped by washing twice with PBS.

SAMD9 and SAMD9L abundance analysis

Transcriptomics and proteomics information of SAMD9 and SAMD9L in different tissues measured for the Cancer Cell Line Encyclopedia (CCLE) was downloaded from the DepMap portal[89]. In brief, Nusinow et al. performed quantitative proteome profiling[90] on 375 CCLE project cell lines in multiplex format with 9 biological samples per plex and one common sample to normalize between plexes. SAMD9 or SAMD9L protein levels data were located and extracted from 262 cell lines. SAMD9 and SAMD9L mRNA expression data normalized in $\log_2$TPM form were downloaded from the DepMap Public 22Q2 Primary Files portal. A heatmap comparing the SAMD9 and SAMD9L mRNA and protein expression levels across CCLE cell lines were plotted in RStudio[91] using R[92] (version 4.2.2), packages dplyr[93] and pheatmap[94].

Phylogenetic analysis of SAMD9 family proteins

The phylogenetic tree was generated with MEGA X software[95]. Briefly, amino acid sequences of SAMD9 and SAMD9L from different species were downloaded from NCBI GenBank. The SAMD9 and SAMD9L multiple sequence alignments were made using ClustalW method with default parameters. The phylogenetic tree was generated by MEGA X using Maximum Likelihood method.

Generation of *Samd9l* knockout mice

To generate KO mice in the C57Bl/6J (The Jackson Laboratory, Strain #: 000664) background, exon 2 of mouse *Samd9l* gene was targeted by two sgRNAs using CRISPR-Cas9 strategy, performed by the Genome Engineering & Stem Cell Center (GESC@MGI) at the Washington University in St. Louis. Briefly, C57Bl/6J female mice were super-ovulated using standard methods and mated with C57Bl/6J male mice. Day 0.5 zygotes were isolated the morning after mating and electroporated with CRISPR reagents (RNPs). Embryos were transferred to pseudo-pregnant recipient females and litters were born. Tails from the pups were sent to GESC for NGS genotyping. Founder animals were identified and bred to establish the lines. The perfect deletion caused 4737-nucleotides elimination in exon 2 of *Samd9l* gene. The *Samd9l* sgRNA sequences used in this study were: ATTTGAAGCTTGAACATGAG and GGCATAAAAGTGATCTAAGG. The genotyping primers used here were: forward primer: 5′-GCAATTGCCTGTGAAATGAGC-3′, reverse primer: 5′-GCCAAGCTCTGTGGTATGGA-3′. All mice were maintained under specific pathogen-free conditions at the Washington University animal facility. Experimental groups included both male and female mice. Animals were housed in ventilated cages with corn cob bedding, fed a standard chow diet, and provided unrestricted access to drinking water. Each cage housed up to five mice and was sanitized weekly within a laminar airflow cabinet. Mice were maintained on a 12-h light/dark cycle to regulate circadian rhythms. Following weaning, whole-body knockout mice were co-housed with wild-type controls from the same facility room, ensuring consistent microbial and environmental conditions throughout the study. All animal experiments adhered to guidelines approved by the Washington University Institutional Animal Care and Use Committee.

Human and mouse ileal organoid cultures

Human intestinal organoids were grown as described below[96]. The murine intestinal organoids were generated according to the protocol described below[97]. Briefly, a 2–3-centimeter segment of ileum was collected from 20-day-old C57Bl/6J or *Samd9l*$^{-/-}$ mice and washed with 20 ml ice-cold PBS once. Tissue was placed into a petri dish with ice-cold PBS, cut longitudinally to expose the lumen, and incubated with 20 ml ice-cold Chelation Buffer (5.6 mM Na_2HPO_4, 8 mM KH_2PO_4, 96.2 mM NaCl, 1.6 mM KCl, 43.4 mM Sucrose, 54.9 mM D-sorbitol, 0.5 mM DL-dithiothreitol) supplemented with 2 mM EDTA for 30 min on ice. After that, the ileal tissue was mixed with 10 ml fresh Chelation Buffer in a 50-ml conical tube and subjected to vigorous shaking for 100 times. The supernatant was collected as fraction 1 (F1). The shaking

process was repeated 4 times to isolate more crypts, and F5 was collected after shaking 500 times. The fractions were filtered through a 70-μm filter separately, pelleted by spinning at 1000×*g* for 10 min at 4 °C, suspended in 50 μl Matrigel matrix (Corning #356234), and seeded in 24-well plates. The isolated organoids were cultured in 600 μl growth medium (50% homemade base medium, 10 μM Rho-associated protein kinase inhibitor (Sigma-Aldrich #688000)) at 37 °C, and the medium was replaced every other day.

Genetic knockout in human intestinal organoids

Genetic knockout in human intestinal organoids was performed as described below[98]. Briefly, human intestinal organoids[83] cultured in Matrigel matrix in 24-well plates were washed once with PBS and then digested by pre-warmed TrypLE Express Enzyme (Gibco #12604013) for 5 min at 37 °C. The digested organoids were pipetted up and down 50 times to fully disperse them into single cells, then mixed with 5 ml Wash Buffer (advanced DMEM F12 medium supplemented with 1× Penicillin-Streptomycin-Glutamine), and pelleted by centrifugation at 1000 rpm for 3 min. After that, cell pellets were resuspended in 500 μl of concentrated lentiviruses encoding Cas9 and sgRNA against *SAMD9* and transferred to a 24-well plate. The plate was centrifuged at 1000 rpm for 60 min at room temperature to facilitate transduction. Afterward, the lentiviruses were carefully removed by pipette, and the organoids were resuspended in 1 ml growth medium (50% homemade base medium, 10 μM Rho-associated protein kinase inhibitor (Sigma-Aldrich #688000)). The organoids were pelleted again at 1000 rpm for 3 min, resuspended in 40 μl Matrigel matrix, seeded in a 24-well plate, and overlaid with 600 μl of growth medium. The medium was changed every other day.

Starting on day 4 post-transduction, the growth medium was supplemented with 2 μg/ml puromycin for 3 weeks. The organoids were routinely split once a week. To select single clonal *SAMD9* KO human intestinal organoids, the pooled *SAMD9* KO organoids were digested into single cells as described above, additionally filtered through a 40-μm strainer (Falcon #352340), and pelleted by spinning at 1000 rpm for 3 min. Afterward, the single cells were resuspended in 1 ml of growth medium, and cell numbers were counted. A total of 500 cells were aliquoted into a 5 ml centrifuge tube, pelleted by centrifugation at 1000 rpm for 3 min, and resuspended in 2.5 ml Matrigel matrix. The Matrigel matrix containing organoids was then seeded at 5 μl per well in five 96-well plates. Each well was filled with 100 μl growth medium, and the medium was changed every other day.

To validate SAMD9 KO by immunofluorescence staining, monolayers were made from single clonal SAMD9 KO human intestinal organoids[96]. Briefly, transwells (Corning #3413) were coated with 100 μl of 33 μg/ml collagen (Sigma-Aldrich #C5533) diluted in ice-cold cell culture-grade water for 1 h at 37 °C. SAMD9 KO organoids cultured in Matrigel matrix were digested using ice-cold 5 μM EDTA (Invitrogen #15575020) by centrifugation at 300×*g* for 3 min, then resuspended in pre-warmed TrypLE Express Enzyme for 20 min in a 37 °C water bath. After digestion, the organoids were dissociated by pipetting up and down 20 times, mixed with 10 ml of Wash Medium, and centrifuged at 300×*g* for 5 min. The supernatant was removed, and the cells were resuspended in 5 ml of Wash Medium, filtered through a 70-μm cell strainer (VWR #76327-100), centrifuged again at 300×*g* for 5 min, and the medium was removed. The cell pellet was resuspended in maintenance medium, and the cell density was determined. The collagen coating was removed from the transwells, and 5×10^5 cells in 100 μl maintenance medium were seeded into the apical compartment of the transwells, while 400 μl of maintenance medium was added to the basolateral compartment. The medium was changed on both sides daily, and differentiation was initiated on day 2 by switching to differentiation medium (50% homemade base medium, 10 μM Y-27632 dihydrochloride, 10 nM Gastrin, 0.5 μM A83-01, 500 nM DAPT, 50 ng/ml human EGF (Invitrogen #A42556)) for an additional 3 days. Poly(dA:dT), LMW poly(I:C) transfection, and immunofluorescence staining were performed as described above.

Rotavirus and *C. parvum* infection and mouse TNF-α stimulation of air-liquid interface mouse ileal organoids

The air-liquid interface ileal organoids were generated based on a previous protocol[99]. Transwells (Corning #3413) were coated with 130 μl 10% Matrigel diluted in ice-cold PBS for 30 min at 37 °C. C57Bl/6J or *Samd9l*$^{-/-}$ ileal organoids grown in 24-well plates were washed with PBS one time and then digested by pre-warmed TrypLE Express Enzyme (Gibco #12604013) for 5 min at 37 °C. The digested organoids were pipetted up and down 50 times to fully disperse the organoids into single cells, which were mixed with 5 ml Wash Buffer (advanced DMEM F12 medium supplemented with 1× Penicillin-Streptomycin-Glutamine), filtered through a 40-μm filter, and pelleted by spinning at 1000 rpm for 3 min. After that, single cells were suspended in 1 ml growth medium, pelleted again by centrifugation at 1000 rpm for 3 min, resuspended in 2 ml growth medium, and seeded into coated transwell (5×10^4 cells) with 400 μl and 130 μl in the bottom and top chambers, respectively. The medium was changed every two days, and the top medium was removed at day 7 to create the air-liquid interface. 3 days later, the organoids were infected with murine rotavirus rD6/2-2g-NSP1-null strain[100] at an MOI of 0.1 by incubating the virus at both bottom and top chambers for 1 h at 37 °C, or incubated with 2×10^5 *Cryptosporidium parvum* AUCP-1 isolate (*C. parvum*)[101] at top chambers for 4 h at 37 °C, or stimulated with 100 ng/ml mouse TNF-α (BioLegend #575202) for 4 h at 37 °C. Then the inoculum in the top was removed, and the bottom was replaced by growth medium supplemented with 0.05 μg/ml trypsin to support RV replication or without trypsin to maintain *C. parvum* infection for another 24 h. For TNF-α stimulation, the inoculum in the top was removed, while the inoculum in the bottom was kept until the samples were harvested at 24 h post-treatment.

Mouse infections

Five-day-old male and female *Samd9l*$^{+/+}$ ($n = 6$) and *Samd9l*$^{-/-}$ ($n = 20$) C57Bl/6J neonatal pups were orally infected with murine RV rD6/2-2g strain[100] or simian RV RRV strain[102] at an inoculum of 1.5×10^3 FFUs or 2.4×10^7 FFUs per mouse, respectively. Diarrhea of rD6/2-2g infected mice was monitored at day 1 post-infection and the fecal specimens from infected mice were also collected. 1.5-ml Eppendorf tubes with 50 μl PBS with Ca^{2+} and Mg^{2+} (Gibco #14040133) were pre-weighted. After stool collection, these tubes were weighted again, and 10 μl of the feces samples (homogenized by Kimble Pellet Pestles (Kimble Chase #749540-0000)) were used for RNA extraction by TRIzol. RNA was reverse-transcribed as described above and an absolute qRT-PCR assay was used to quantify the genome copy numbers of RV in the stool. A standard curve was generated by Taqman assays using the RV NSP5 primers aforementioned with the pT7-D6/2-NSP5[100] plasmid as input to normalize CT values to RV genome copy numbers. Jejunum, ileum, and lung of RRV inoculated mice were collected at day 3 post-infection. RNA was extracted from those tissues using RNeasy Mini Kit following the manufacturer's protocol. The RV NSP5 mRNA levels were measured by qRT-PCR as described above.

To monitor the diarrhea, biliary disease, and lethality[56] caused by a virulent reovirus T3SA$^+$ strain[103], 3-day-old *Samd9l*$^{+/+}$ ($n = 20$) and *Samd9l*$^{-/-}$ ($n = 19$) neonatal pups, including both male and female, were intraperitoneal (IP) injected with 1×10^4 PFUs of T3SA$^+$. Diarrheal, biliary diseases, and mortality were monitored as mentioned above from days 1 to 15 post-infection. Spleen, liver, kidney, lung, heart, and brain of reovirus-infected mice were collected at day 9 post-infection. RNA was extracted from those tissues using RNeasy Mini Kit following the manufacturer's protocol. The reovirus T1F mRNA levels were measured by qRT-PCR as described above.

For euthanasia, suckling pups were either directly decapitated or placed in a Bell jar with a grate floor, and sufficient isoflurane was

applied to the absorbent material to achieve a concentration of at least 10%. Mice remained in the chamber for a minimum of 60 s after cessation of respiration, after which critical organs were harvested to ensure death.

Generation of recombinant RVs by a plasmid-based reverse genetics system

To generate pT7-SA11-ΔNSP1, pT7-SA11-NSP1-ΔC17, and pT7-SA11-ΔNSP6 plasmids, CATTAT codons at nucleotide position 28 to 33 in the SA11-NSP1 open reading frame (ORF), ACTTTA codons at nucleotide position 1435 to 1440 in the SA11-NSP1 ORF, or ATGATT codons at the nucleotide position 1 to 6 in the SA11-NSP6 ORF, were replaced with premature stop codons TAATAG, Isoleucine and stop codons ATTTAA, or threonine ACGACT, using QuikChange II site-directed mutagenesis kit, based on pT7-SA11-NSP1 or pT7-SA11-NSP5 plasmids[104], separately. The recombinant simian RV SA11-ΔNSP1, SA11-NSP1-ΔC17, and SA11-ΔNSP6 were rescued based on previous protocol[60]. Briefly, BHK-T7 cells (2×10^5) in 12-well plates were transfected with 0.4 μg of pT7-SA11-VP1, pT7-SA11-VP2, pT7-SA11-VP3, pT7-SA11-VP4, pT7-SA11-VP6, pT7-SA11-VP7, pT7-SA11-NSP1 (or pT7-SA11-ΔNSP1, pT7-SA11-NSP1-ΔC17), pT7-SA11-NSP3, pT7-SA11-NSP4; 1.2 μg of pT7-SA11-NSP2 and pT7-SA11-NSP5 (or pT7-SA11-ΔNSP6); 0.8 μg of helper plasmid C3P3-G1; and 14 μl TransIT-LT1 transfection reagent (Mirus #MIR2305) for 18 h. Then the transfected cells were washed with serum-free DMEM medium for two times, and grown in 800 μl serum-free DMEM for another 24 h. After that, 5×10^4 MA104-N*V cells in 200 μl serum-free DMEM medium were added to the BHK-T7 cells, with additional trypsin at the final concentration of 0.5 μg/ml. Three days later, the cells were frozen and thawed three times to harvest rescued virus, and this virus was propagated in MA104 cells in 6-well plates one time, then the virus was used to propagate in T75 flasks to generate the virus stock.

Inhibitor screening assay

To test the potential signaling pathway involved in RV-NSP1 caused decreased protein level of SAMD9, HEK293 cells (1×10^5) in 24-well plates were co-transfected with SAMD9-Myc-DDK (0.5 μg) and pG-LAP6-ev/Wa-NSP1 (0.5 μg) for 36 h, then the cells were treated with the cell-permeable 26S proteasome inhibitors MG132 (Selleckchem #S2619, 10 μM), PYR-41 (Selleckchem #S7129, 50 μM), and bortezomib (Selleckchem #S1013, 10 μM), or the NEDD8-activating enzyme inhibitor MLN4924 (Selleckchem #S7109, 10 μM) for another 12 h.

siRNA transfection

siRNA reverse transfection assay was performed as described below[75]. Briefly, 1 μl of 5 μM control siRNA (Dharmacon #D-001810-10-05) or human NEDD8 siRNA SMARTPool (Dharmacon #L-020081-00-0005) was mixed with 5 μl RNAiMAX (Invitrogen #13778100) in 50 μl Opti-MEM (Gibco #11058021), incubated in 24-well plates for 20 min at room temperature. Then HEK293 cells (5×10^4) resuspended in antibiotic-free complete medium were added to the plates. 48 h later, the siRNA-transfected cells were co-transfected with SAMD9-Myc-DDK and pG-LAP6-ev/Wa-NSP1 for 36 h as described above.

Flow cytometry

To cross-examine the SAMD9 or SAMD9L from different species targeted by different RVs NSP1s, *SAMD9* KO HEK293 cells (1×10^5) in 24-well plates were co-transfected with hSAMD9, hSAMD9L, mSAMD9L-C57Bl/6, mSAMD9L-129sv, hmSAMD9, hmSAMD9L, or zSAMD9L and pG-LAP6-ev, Wa-NSP1, ST3-NSP1, ETD-NSP1, or UK-NSP1 for 48 h. The transfected cells were washed three times with PBS and trypsin lysed to single cells. 3×10^4 cells were resuspended in 100 μl PBS supplemented with Zombie Aqua (BioLegend #423101, 1:2000) and incubated for 30 min at room temperature, then the cells were washed twice with PBS. Next, the cells were fixed in 100 μl Cytofix/Cytoperm solution (BD #554722) for 20 min on ice, and washed twice by 200 μl Perm/Wash buffer (BD #554723). The fixed cells were incubated with APC anti-DYKDDDDK tag antibody (BioLegend #637308, 1:500) diluted in 50 μl Perm/Wash buffer for 1 h at room temperature, and washed three times with 200 μl Pem/Wash buffer. The samples were obtained on Sartorius iQue 3 Advanced Flow Cytometry and analyzed by the FlowJo software 10.8.1.

Human Institutional Review Board approval

The collection and use of human tissue for establishing primary cell culture or organoid culture were approved by the Washington University Human Research Protection Office (IRB #201404112) and collected with written informed consent by the Washington University Digestive Diseases Research Core Center Biobank Core.

Statistical analyses

Prism 10.3.0 (GraphPad) was used to perform statistical analyses. Error bars (mean values with SEM) and sample size for each experiment are defined in the figure legends.

Reporting summary

Further information on research design is available in the Nature Portfolio Reporting Summary linked to this article.

Data availability

RNA sequencing dataset is deposited at the NCBI Gene Expression Omnibus (GSE228684: [https://www.ncbi.nlm.nih.gov/geo/query/acc.cgi?acc=GSE228684]). All data are included in the Supplementary Information or available from the authors, as are unique reagents used in this article. All relevant data are available from the paper or from the authors upon request. Source data are provided with this paper.

References

1. Iwasaki, A. & Medzhitov, R. Control of adaptive immunity by the innate immune system. *Nat. Immunol.* **16**, 343–353 (2015).
2. Fitzgerald, K. A. & Kagan, J. C. Toll-like receptors and the control of immunity. *Cell* **180**, 1044–1066 (2020).
3. Sun, L., Wu, J., Du, F., Chen, X. & Chen, Z. J. Cyclic GMP-AMP synthase is a cytosolic DNA sensor that activates the type I interferon pathway. *Science* **339**, 786–791 (2013).
4. Wu, J. et al. Cyclic GMP-AMP is an endogenous second messenger in innate immune signaling by cytosolic DNA. *Science* **339**, 826–830 (2013).
5. Yoneyama, M. et al. The RNA helicase RIG-I has an essential function in double-stranded RNA-induced innate antiviral responses. *Nat. Immunol.* **5**, 730–737 (2004).
6. Kang, D.-c. et al. mda-5: an interferon-inducible putative RNA helicase with double-stranded RNA-dependent ATPase activity and melanoma growth-suppressive properties. *Proc. Natl Acad. Sci. USA* **99**, 637–642 (2002).
7. Hornung, V. et al. 5′-Triphosphate RNA is the ligand for RIG-I. *Science* **314**, 994–997 (2006).
8. Goubau, D. et al. Antiviral immunity via RIG-I-mediated recognition of RNA bearing 5′-diphosphates. *Nature* **514**, 372–375 (2014).
9. Kato, H. et al. Differential roles of MDA5 and RIG-I helicases in the recognition of RNA viruses. *Nature* **441**, 101–105 (2006).
10. Seth, R. B., Sun, L., Ea, C. K. & Chen, Z. J. Identification and characterization of MAVS, a mitochondrial antiviral signaling protein that activates NF-kappaB and IRF 3. *Cell* **122**, 669–682 (2005).
11. Kawai, T. et al. IPS-1, an adaptor triggering RIG-I- and Mda5-mediated type I interferon induction. *Nat. Immunol.* **6**, 981–988 (2005).
12. Meylan, E. et al. Cardif is an adaptor protein in the RIG-I antiviral pathway and is targeted by hepatitis C virus. *Nature* **437**, 1167–1172 (2005).

13. Xu, L. G. et al. VISA is an adapter protein required for virus-triggered IFN-beta signaling. *Mol. Cell* **19**, 727–740 (2005).
14. Bauernfried, S., Scherr, M. J., Pichlmair, A., Duderstadt, K. E. & Hornung, V. Human NLRP1 is a sensor for double-stranded RNA. *Science*. https://doi.org/10.1126/science.abd0811 (2021).
15. Unterholzner, L. et al. IFI16 is an innate immune sensor for intracellular DNA. *Nat. Immunol.* **11**, 997–1004 (2010).
16. Liddicoat, B. J. et al. RNA editing by ADAR1 prevents MDA5 sensing of endogenous dsRNA as nonself. *Science* **349**, 1115–1120 (2015).
17. Balachandran, S. et al. Essential role for the dsRNA-dependent protein kinase PKR in innate immunity to viral infection. *Immunity* **13**, 129–141 (2000).
18. Fernandes-Alnemri, T., Yu, J. W., Datta, P., Wu, J. & Alnemri, E. S. AIM2 activates the inflammasome and cell death in response to cytoplasmic DNA. *Nature* **458**, 509–513 (2009).
19. Takaoka, A. et al. DAI (DLM-1/ZBP1) is a cytosolic DNA sensor and an activator of innate immune response. *Nature* **448**, 501–505 (2007).
20. Jiao, H. et al. Z-nucleic-acid sensing triggers ZBP1-dependent necroptosis and inflammation. *Nature* **580**, 391–395 (2020).
21. Schoggins, J. W. et al. Pan-viral specificity of IFN-induced genes reveals new roles for cGAS in innate immunity. *Nature* **505**, 691–695 (2014).
22. Knight, M. J., Leettola, C., Gingery, M., Li, H. & Bowie, J. U. A human sterile alpha motif domain polymerizome. *Protein Sci.* **20**, 1697–1706 (2011).
23. Peng, S. et al. Structure and function of an effector domain in antiviral factors and tumor suppressors SAMD9 and SAMD9L. *Proc. Natl Acad. Sci. USA* **119**, e2116550119 (2022).
24. Mekhedov, S. L., Makarova, K. S. & Koonin, E. V. The complex domain architecture of SAMD9 family proteins, predicted STAND-like NTPases, suggests new links to inflammation and apoptosis. *Biol. Direct* **12**, 13 (2017).
25. Liu, J., Wennier, S., Zhang, L. & McFadden, G. M062 is a host range factor essential for myxoma virus pathogenesis and functions as an antagonist of host SAMD9 in human cells. *J. Virol.* **85**, 3270–3282 (2011).
26. Sivan, G., Ormanoglu, P., Buehler, E. C., Martin, S. E. & Moss, B. Identification of restriction factors by human genome-wide RNA interference screening of viral host range mutants exemplified by discovery of SAMD9 and WDR6 as inhibitors of the vaccinia virus K1L^{-}C7L^{-} mutant. *mBio* **6**, e01122 (2015).
27. Meng, X. et al. A paralogous pair of mammalian host restriction factors form a critical host barrier against poxvirus infection. *PLoS Pathog.* **14**, e1006884 (2018).
28. Lemos de Matos, A., Liu, J., McFadden, G. & Esteves, P. J. Evolution and divergence of the mammalian SAMD9/SAMD9L gene family. *BMC Evol. Biol.* **13**, 121 (2013).
29. Narumi, S. et al. SAMD9 mutations cause a novel multisystem disorder, MIRAGE syndrome, and are associated with loss of chromosome 7. *Nat. Genet.* **48**, 792–797 (2016).
30. Li, C. F. et al. Human sterile alpha motif domain 9, a novel gene identified as down-regulated in aggressive fibromatosis, is absent in the mouse. *BMC Genom.* **8**, 1–17 (2007).
31. Crawford, S. E. et al. Rotavirus infection. *Nat. Rev. Dis. Prim.* **3**, 17083 (2017).
32. Dermody, T., Parker, J. & Sherry, B. Orthoreoviruses (Lippincott Williams & Wilkins, 2013).
33. Aliabadi, N. et al. Global impact of rotavirus vaccine introduction on rotavirus hospitalisations among children under 5 years of age, 2008-16: findings from the Global Rotavirus Surveillance Network. *Lancet Glob. Health* **7**, e893–e903 (2019).
34. Bouziat, R. et al. Reovirus infection triggers inflammatory responses to dietary antigens and development of celiac disease. *Science* **356**, 44–50 (2017).
35. Deal, E. M., Jaimes, M. C., Crawford, S. E., Estes, M. K. & Greenberg, H. B. Rotavirus structural proteins and dsRNA are required for the human primary plasmacytoid dendritic cell IFNα response. *PLoS Pathog.* **6**, e1000931 (2010).
36. Fernández de Castro, I. et al. Reovirus forms neo-organelles for progeny particle assembly within reorganized cell membranes. *mBio* **5**, e00931–13 (2014).
37. Ding, S. et al. Rotavirus VP3 targets MAVS for degradation to inhibit type III interferon expression in intestinal epithelial cells. *Elife*. https://doi.org/10.7554/eLife.39494 (2018).
38. Zurney, J., Kobayashi, T., Holm, G. H., Dermody, T. S. & Sherry, B. Reovirus mu2 protein inhibits interferon signaling through a novel mechanism involving nuclear accumulation of interferon regulatory factor 9. *J. Virol.* **83**, 2178–2187 (2009).
39. Andrejeva, J. et al. The V proteins of paramyxoviruses bind the IFN-inducible RNA helicase, mda-5, and inhibit its activation of the IFN-beta promoter. *Proc. Natl Acad. Sci. USA* **101**, 17264–17269 (2004).
40. Zhang, F. et al. Human SAMD9 is a poxvirus-activatable anticodon nuclease inhibiting codon-specific protein synthesis. *Sci. Adv.* **9**, eadh8502 (2023).
41. Haag, S. M. et al. Targeting STING with covalent small-molecule inhibitors. *Nature* **559**, 269–273 (2018).
42. Ablasser, A. et al. RIG-I-dependent sensing of poly(dA:dT) through the induction of an RNA polymerase III–transcribed RNA intermediate. *Nat. Immunol.* **10**, 1065–1072 (2009).
43. Lafont, E. et al. TBK1 and IKKε prevent TNF-induced cell death by RIPK1 phosphorylation. *Nat. Cell Biol.* **20**, 1389–1399 (2018).
44. Harrison, C. et al. JAK inhibition with ruxolitinib versus best available therapy for myelofibrosis. *N. Engl. J. Med.* **366**, 787–798 (2012).
45. Rappe, J. C. F. et al. A TLR7 antagonist restricts interferon-dependent and -independent immunopathology in a mouse model of severe influenza. *J. Exp. Med*. https://doi.org/10.1084/jem.20201631 (2021).
46. Conrad, S. J. et al. Myxoma virus lacking the host range determinant M062 stimulates cGAS-dependent type 1 interferon response and unique transcriptomic changes in human monocytes/macrophages. *PLoS Pathog.* **18**, e1010316 (2022).
47. Zhang, X. et al. The cytosolic DNA sensor cGAS forms an oligomeric complex with DNA and undergoes switch-like conformational changes in the activation loop. *Cell Rep.* **6**, 421–430 (2014).
48. Kowalinski, E. et al. Structural basis for the activation of innate immune pattern-recognition receptor RIG-I by viral RNA. *Cell* **147**, 423–435 (2011).
49. Jiang, F. et al. Structural basis of RNA recognition and activation by innate immune receptor RIG-I. *Nature* **479**, 423–427 (2011).
50. Peisley, A. et al. Kinetic mechanism for viral dsRNA length discrimination by MDA5 filaments. *Proc. Natl Acad. Sci. USA* **109**, E3340–E3349 (2012).
51. Crawford, S. E., Ding, S., Greenberg, H. B. & Estes, M. K. *Fields Virology* 7th edn (Lippincott Williams & Wilkins, 2022).
52. Nounamo, B. et al. An interaction domain in human SAMD9 is essential for myxoma virus host-range determinant M062 antagonism of host anti-viral function. *Virology* **503**, 94–102 (2017).
53. Pappas, D. J. et al. Longitudinal system-based analysis of transcriptional responses to type I interferons. *Physiol. Genomics* **38**, 362–371 (2009).
54. Li, C. F. et al. Human sterile alpha motif domain 9, a novel gene identified as down-regulated in aggressive fibromatosis, is absent in the mouse. *BMC Genomics* **8**, 92 (2007).
55. Boon, A. C., Williams, R. W., Sinasac, D. S. & Webby, R. J. A novel genetic locus linked to pro-inflammatory cytokines after virulent H5N1 virus infection in mice. *BMC Genomics* **15**, 1017 (2014).
56. Barton, E. S. et al. Utilization of sialic acid as a coreceptor is required for reovirus-induced biliary disease. *J. Clin. Invest.* **111**, 1823–1833 (2003).

57. Deng, S. et al. *Cryptosporidium* uses CSpV1 to activate host type I interferon and attenuate antiparasitic defenses. *Nat. Commun.* **14**, 1456 (2023).
58. Willemsen, J. et al. TNF leads to mtDNA release and cGAS/STING-dependent interferon responses that support inflammatory arthritis. *Cell Rep.* **37**, 109977 (2021).
59. Antia, A., Pinski, A. N. & Ding, S. Re-examining rotavirus innate immune evasion: potential applications of the reverse genetics system. *mBio* **13**, e0130822 (2022).
60. Sánchez-Tacuba, L. et al. An optimized reverse genetics system suitable for efficient recovery of simian, human, and murine-like rotaviruses. *J. Virol.* https://doi.org/10.1128/jvi.01294-20 (2020).
61. Zhao, B. et al. Structural basis for concerted recruitment and activation of IRF-3 by innate immune adaptor proteins. *Proc. Natl Acad. Sci. USA* **113**, E3403–E3412 (2016).
62. Soucy, T. A. et al. An inhibitor of NEDD8-activating enzyme as a new approach to treat cancer. *Nature* **458**, 732–736 (2009).
63. Liu, J. & McFadden, G. SAMD9 is an innate antiviral host factor with stress response properties that can be antagonized by poxviruses. *J. Virol.* **89**, 1925–1931 (2015).
64. Meng, X. & Xiang, Y. RNA granules associated with SAMD9-mediated poxvirus restriction are similar to antiviral granules in composition but do not require TIA1 for poxvirus restriction. *Virology* **529**, 16–22 (2019).
65. Schoggins, J. W. Interferon-stimulated genes: what do they all do? *Annu. Rev. Virol.* **6**, 567–584 (2019).
66. Sivan, G., Ormanoglu, P., Buehler, E. C., Martin, S. E. & Moss, B. Identification of restriction factors by human genome-wide RNA interference screening of viral host range mutants exemplified by discovery of SAMD9 and WDR6 as inhibitors of the vaccinia virus K1L-C7L- mutant. *mBio* **6**, e01122 (2015).
67. Zhang, F., Meng, X., Townsend, M. B., Satheshkumar, P. S. & Xiang, Y. Identification of CP77 as the third orthopoxvirus SAMD9 and SAMD9L inhibitor with unique specificity for a rodent SAMD9L. *J. Virol.* https://doi.org/10.1128/jvi.00225-19 (2019).
68. Acharya, D. et al. Actin cytoskeleton remodeling primes RIG-I-like receptor activation. *Cell* **185**, 3588–3602.e3521 (2022).
69. Mu, X. et al. Cytoskeleton stiffness regulates cellular senescence and innate immune response in Hutchinson-Gilford Progeria Syndrome. *Aging Cell* **19**, e13152 (2020).
70. Ledvina, H. E. et al. An E1-E2 fusion protein primes antiviral immune signalling in bacteria. *Nature* https://doi.org/10.1038/s41586-022-05647-4 (2023).
71. Jenson, J. M., Li, T., Du, F., Ea, C. K. & Chen, Z. J. Ubiquitin-like conjugation by bacterial cGAS enhances anti-phage defence. *Nature* https://doi.org/10.1038/s41586-023-05862-7 (2023).
72. Gao, D. et al. Cyclic GMP-AMP synthase is an innate immune sensor of HIV and other retroviruses. *Science* **341**, 903–906 (2013).
73. Gao, D. et al. Activation of cyclic GMP-AMP synthase by self-DNA causes autoimmune diseases. *Proc. Natl Acad. Sci. USA* **112**, E5699–E5705 (2015).
74. Abdelhamed, S. et al. Mutant Samd9l expression impairs hematopoiesis and induces bone marrow failure in mice. *J. Clin. Invest.* https://doi.org/10.1172/jci158869 (2022).
75. Ding, S. et al. Comparative proteomics reveals strain-specific β-TrCP degradation via rotavirus NSP1 hijacking a host Cullin-3-Rbx1 complex. *PLoS Pathog.* **12**, e1005929 (2016).
76. Dobin, A. et al. STAR: ultrafast universal RNA-seq aligner. *Bioinformatics* **29**, 15–21 (2013).
77. Liao, Y., Smyth, G. K. & Shi, W. featureCounts: an efficient general purpose program for assigning sequence reads to genomic features. *Bioinformatics* **30**, 923–930 (2014).
78. Patro, R., Duggal, G., Love, M. I., Irizarry, R. A. & Kingsford, C. Salmon provides fast and bias-aware quantification of transcript expression. *Nat. Methods* **14**, 417–419 (2017).
79. Wang, L., Wang, S. & Li, W. RSeQC: quality control of RNA-seq experiments. *Bioinformatics* **28**, 2184–2185 (2012).
80. Love, M. I., Huber, W. & Anders, S. Moderated estimation of fold change and dispersion for RNA-seq data with DESeq2. *Genome Biol.* **15**, 550 (2014).
81. Langfelder, P. & Horvath, S. WGCNA: an R package for weighted correlation network analysis. *BMC Bioinform.* **9**, 559 (2008).
82. Song, Y. et al. Inhibitor of growth protein 3 epigenetically silences endogenous retroviral elements and prevents innate immune activation. *Nucleic Acids Res.* **49**, 12706–12715 (2021).
83. Zang, R. et al. TMPRSS2 and TMPRSS4 promote SARS-CoV-2 infection of human small intestinal enterocytes. *Sci. Immunol.* **5**, eabc3582 (2020).
84. Shen, C. et al. Phase separation drives RNA virus-induced activation of the NLRP6 inflammasome. *Cell* **184**, 5759–5774.e5720 (2021).
85. Weber, M. & Weber, F. Monitoring activation of the antiviral pattern recognition receptors RIG-I and PKR by limited protease digestion and native PAGE. *J. Vis. Exp.* https://doi.org/10.3791/51415 (2014).
86. Komoto, S. et al. Generation of recombinant rotaviruses expressing fluorescent proteins by using an optimized reverse genetics system. *J. Virol.* https://doi.org/10.1128/jvi.00588-18 (2018).
87. Sharon, R. et al. α-Synuclein occurs in lipid-rich high molecular weight complexes, binds fatty acids, and shows homology to the fatty acid-binding proteins. *Proc. Natl Acad. Sci. USA* **98**, 9110–9115 (2001).
88. Li, X. & Donowitz, M. Fractionation of subcellular membrane vesicles of epithelial and nonepithelial cells by OptiPrep™ density gradient ultracentrifugation. *Methods Mol. Biol.* **440**, 97–110 (2008).
89. Ghandi, M. et al. Next-generation characterization of the cancer cell line encyclopedia. *Nature* **569**, 503–508 (2019).
90. Nusinow, D. P. et al. Quantitative proteomics of the cancer cell line encyclopedia. *Cell* **180**, 387–402.e316 (2020).
91. Allaire, J. RStudio: integrated development environment for R. Available at https://posit.co/download/rstudio-desktop/ (2012).
92. R Core Team. R: a language and environment for statistical computing. Available at https://cran.r-project.org/ (2013).
93. Wickham, H., François, R., Henry, L. & Müller, K. dplyr: a grammar of data manipulation. R package version 0.4. Available at https://dplyr.tidyverse.org/ (2015).
94. Kolde, R. pheatmap: pretty heatmaps. R. package version 1. Available at https://cran.r-project.org/web/packages/pheatmap/index.html (2012).
95. Hall, B. G. Building phylogenetic trees from molecular data with MEGA. *Mol. Biol. Evol.* **30**, 1229–1235 (2013).
96. Ding, S. et al. Retinoic acid and lymphotoxin signaling promote differentiation of human intestinal M cells. *Gastroenterology* **159**, 214–226.e211 (2020).
97. Sato, T. et al. Long-term expansion of epithelial organoids from human colon, adenoma, adenocarcinoma, and Barrett's epithelium. *Gastroenterology* **141**, 1762–1772 (2011).
98. Lin, S. C., Haga, K., Zeng, X. L. & Estes, M. K. Generation of CRISPR-Cas9-mediated genetic knockout human intestinal tissue-derived enteroid lines by lentivirus transduction and single-cell cloning. *Nat. Protoc.* **17**, 1004–1027 (2022).
99. Wilke, G. et al. A stem-cell-derived platform enables complete *Cryptosporidium* development in vitro and genetic tractability. *Cell Host Microbe* **26**, 123–134.e128 (2019).
100. Hou, G., Zeng, Q., Matthijnssens, J., Greenberg, H. B. & Ding, S. Rotavirus NSP1 contributes to intestinal viral replication, pathogenesis, and transmission. *mBio* **12**, e0320821 (2021).
101. Kuhlenschmidt, T. B. et al. Inhibition of calcium-dependent protein kinase 1 (CDPK1) in vitro by pyrazolopyrimidine derivatives does

not correlate with sensitivity of *Cryptosporidium parvum* growth in cell culture. *Antimicrob. Agents Chemother.* **60**, 570–579 (2016).
102. Gombold, J. L. & Ramig, R. F. Analysis of reassortment of genome segments in mice mixedly infected with rotaviruses SA11 and RRV. *J. Virol.* **57**, 110–116 (1986).
103. Holm, G. H. et al. Interferon regulatory factor 3 attenuates reovirus myocarditis and contributes to viral clearance. *J. Virol.* **84**, 6900–6908 (2010).
104. Kanai, Y. et al. Entirely plasmid-based reverse genetics system for rotaviruses. *Proc. Natl Acad. Sci. USA* **114**, 2349–2354 (2017).

Acknowledgements

We thank all members of the Ding laboratory, Drs. Liang Shan and Megan Baldridge (WUSTL), Dr. Jan Carette (Stanford University), and Dr. Mary Estes (Baylor College of Medicine) for helpful discussions. We also thank Dr. Jacco Boon (WUSTL) for the hamster tissue, Dr. Diane Sepich (WUSTL) for the zebrafish tissue, Dr. Peter Bayguinov (WUSTL, WUCCI) for his assistance with the super-resolution microscope, and the WUSTL GTAC core for their help with the RNA sequencing. We thank the Genome Engineering & Stem Cell Center (GESC@MGI) at WUSTL for reagent validation services of generating *Samd9l*$^{-/-}$ mice. Mass Spectrometry analyses were performed by the Mass Spectrometry Technology Access Center at the McDonnell Genome Institute (MTAC@MGI) at Washington University School of Medicine, supported by the Diabetes Research Center/NIH grant P30 DK020579, Institute of Clinical and Translational Sciences/NCATS CTSA award UL1 TR002345, and Siteman Cancer Center/NCI CCSG grant P30 CA091842. G.H. is supported in part by a Stephen I. Morse Fellowship. This work was supported by R01 AI139106, VCRI grant (UAMS), ABI-VCRI grant (UA), and River Valley Ovarian Cancer Coalition to J.L., R01 AI174526 to T.S.D., and K99/R00 AI135031, R01 AI150796, and U19 AI116484 to S.D.

Author contributions

S.D. conceived the study. G.H. performed all experiments with help from L.R. and C.L. W.B. performed the negative staining assay. S.D., J.S., J.L., and G.H. constructed the knockout cells. S.D., Y.S.O., Y.Z., and G.H. performed the virus infections. J.L. performed the monkeypox virus infection. W.H. performed the cryptosporidium infection. O.L.W. and D.M.S. prepared and determined titers of reovirus stocks. D.L. analyzed the abundance of SAMD9 and SAMD9L in different tissues. Q.S. and C.S. purified SAMD9 proteins. G.H. and C.L. constructed the phylogenetic tree of SAMD9 and SAMD9L. T.S.D., C.S., J.L., and L.D.S. contributed critical reagents and input on the study. S.D. and G.H. composed the manuscript. All authors reviewed and edited the manuscript.

Competing interests

The authors declare no competing interests.

Additional information

Supplementary information The online version contains supplementary material available at https://doi.org/10.1038/s41467-025-59090-w.

Correspondence and requests for materials should be addressed to Siyuan Ding.

Peer review information *Nature Communications* thanks the anonymous reviewer(s) for their contribution to the peer review of this work. A peer review file is available.